

Superconducting order parameter manifested in quasicrystals

Sougata Biswas ^{1,*}, Debika Debnath ^{1,†} and Paramita Dutta ^{1,‡}

¹*Theoretical Physics Division, Physical Research Laboratory, Navrangpura, Ahmedabad-380009, India*

Recent discovery of the superconducting ground state in Quasicrystals (QCs) has opened up an exciting new avenue for superconductivity based on QCs. However, theoretical studies to date have largely focused on a limited subset of quasiperiodic structures. In this work, we broaden the scope by theoretically investigating the behavior of the superconducting order parameter (OP) across a wide class of aperiodic systems, including both generalized Fibonacci and non-Fibonacci QCs based on the attractive Hubbard model. We begin with a one-dimensional toy model, and for the generality of our findings, we extend our analysis to two-dimensional QCs. Remarkably, despite the increased dimensionality, the qualitative features of the OP remain largely preserved. By systematically analyzing models generated through various growth rules, we elucidate the influence of quasiperiodicity on the OP amplitudes. We study the evolution of the OP with respect to the temperature, strength of the interaction, and nearest-neighbor hopping amplitude. Our numerical analysis identifies the most favorable QC structure and parameter regime that supports enhanced onsite pairing amplitudes. Additionally, we provide a comparative analysis of the superconducting transition temperatures across the range of quasiperiodic configurations. To gain further insight into these systems, we compute key thermodynamic quantities: the entropy and electronic specific heat, and examine their dependence on the underlying structural sequences. This analysis enables us to determine which QC structures are most conducive to Cooper pair formation.

I. INTRODUCTION

The discovery of metallic phases in materials that lack translational symmetry but exhibit long-range orientational order, known as quasicrystals (QCs), has opened an exciting new frontier in condensed matter physics research in 1984 [1]. Although QCs do not possess the periodicity found in regular crystals, their atomic arrangements follow deterministic rules that establish long-range order into its configuration [2–4]. In regular crystals with perfect periodicity, electron wavefunctions typically extend throughout the lattice, leading to metallic behavior, whereas in disordered systems, wavefunctions become mostly localized, exhibiting an insulating phase. Interestingly, QCs offer a rich landscape for the spectral and wave function’s behavior. The eigenstates are neither fully localized nor fully extended in QCs [3–8]. These are critical states that feature unique spatial structures characterized by multifractal scaling. QCs often exhibit energy spectra resembling a Cantor set [3, 6, 9–11], offering a testing ground for exploring unusual transport and localization phenomena [12–15]. QCs have been realized experimentally using the fabrication of multilayered structures [16–30].

The long-range ordering in QCs manifests in various sequences or patterns depending on the dimension of the system. Among one-dimensional (1D) QCs, Fibonacci quasiperiodicity is the most well-known structure where the number of sites or bonds in successive generations grows according to the Fibonacci sequence. The classic Fibonacci sequence can be generalized by extend-

ing the recurrence relations, giving rise to the generalized Fibonacci QCs (GFQCs). Along with GFQCs, other 1D quasiperiodic sequences such as Thue-Morse, period-doubling, approximant QCs etc. have emerged as prototypical models for exploring the interplay between quasiperiodicity and various quantum mechanical properties [22, 31–46]. These systems have been extensively investigated, particularly in relation to their spectral characteristics, thermodynamic properties, and wave function behavior [37, 47–55]. In addition to static and spectral characteristics, significant attention has been devoted to understanding the quantum dynamics in QCs [56–64], enriching the study on these systems as a bridge between regular crystals and disordered materials.

Recent works on QCs have renewed the interest of the community in a new way. Topological phases have been shown to appear in QCs, extending the concept beyond the conventional paradigm of metal-insulator phases [65–70]. The possibility of boundary states in the topological phases makes them an important platform for exploring quantum phases of matter [71–79]. On top of that, the recent discovery of superconducting ground state in Fibonacci QC and their approximants based on the Al–Zn–Mg alloy has marked a possibility of QC-based superconductivity [80]. This recent discovery highlighted the relevance of quasiperiodic structures for realizing novel superconducting phases. There is no exception from the previous trend that Fibonacci QCs are taken as the first test ground for superconductivity, too, as it is one of the simplest and most well-understood models of 1D quasiperiodicity, which can provide a valuable framework for exploring fundamental physical phenomena. The superconducting properties of Fibonacci QCs have been explored to understand how the absence of translational symmetry influences superconducting pair-

* sougatabiswas@prl.res.in

† debika.uoh@gmail.com

‡ paramita@prl.res.in

ing [81–86]. Superconductivity has also been reported in some two-dimensional (2D) QCs based on the Penrose and Ammann-Beenker tiling [87–90]. These studies have revealed that quasiperiodic order can give rise to both conventional and unconventional superconducting phases where the superconducting gap and the local pairing amplitude exhibit non-uniform, often fractal-like spatial profiles. It also includes the appearance of topological superconductivity [84, 87, 91].

The emergence of superconductivity and the corresponding behavior of the pairing amplitude have been extensively investigated across a wide variety of periodic lattice systems, including those subjected to various forms of disorder [92–104]. However, a natural question appears here: what happens in other QCs, particularly with more complex structures? Addressing these questions is indeed required to gain a broader and deeper understanding of how different types of quasiperiodic orders affect superconducting properties. This naturally raises the question: given that different quasiperiodic structures have different construction patterns and exhibit distinct spectral characteristics, do their superconducting properties also vary accordingly? How to find the best candidate for the Cooper pair formation within the QC zoo? Motivated by these fundamental questions, we present a detailed study on the superconducting order parameter (OP) in a variety of QCs considering various quasiperiodic orders. We start with 1D toy models and then extend our analysis to 2D QCs from the realistic point of view. We take a few examples from the GFQC family corresponding to the two different subclasses, namely, subclass-I and subclass-II. As a prototype, we consider Fibonacci, Silver-mean, and Bronze-mean QCs from subclass-I and Copper-mean and Nickel-mean QCs from subclass-II as mentioned in Table-I. For examples from other than GFQCs, we study the Thue-Morse and Period-doubling QCs (see Table-I) which differ significantly in their local environments, hierarchical structure, and spectral characteristics from the GFQCs [105, 106]. Important questions arise about the universality or variability of key features, such as the spatial pattern of the OP, the temperature dependence of the OP, and their thermodynamic properties.

The primary goal of our study is to understand the origin of the behavior of the OP across the range of QCs we examine. We find that while each sequence exhibits spatial variation in the OP, these patterns and their magnitudes are not universal; instead, they strongly depend on the underlying sequence and the range of parameters governing the generation of the sequence. Using an attractive Hubbard model, we investigate how the OP distributions evolve with quasiperiodicity. We also provide a comparative analysis to identify the conditions favorable for Cooper pair formation. We show that OP amplitudes are strongly sensitive to the sequences of the QCs and also to the model parameters. The transition temperatures vary largely with the configurations and parameter values of the QCs as well. Our findings offer guidelines

TABLE I. Growth Rules of GFQC (subclass-I and II) and non-GFQCs.

Class	QCs	Growth Rules
GFQC-I	Fibonacci	$t_A \rightarrow t_A t_B, t_B \rightarrow t_A$
	Silver-mean	$t_A \rightarrow t_A t_A t_B, t_B \rightarrow t_A$
	Bronze-mean	$t_A \rightarrow t_A t_A t_A t_B, t_B \rightarrow t_A$
GFQC-II	Copper-mean	$t_A \rightarrow t_A t_B t_B, t_B \rightarrow t_A$
	Nickel-mean	$t_A \rightarrow t_A t_B t_B t_B, t_B \rightarrow t_A$
Non-GFQC	Thue-Morse	$t_A \rightarrow t_A t_B, t_B \rightarrow t_B t_A$
	Period-doubling	$t_A \rightarrow t_A t_B, t_B \rightarrow t_A t_A$

for a broad class of aperiodic systems to identify which QC is the best choice for higher OP, with potential implications spanning from condensed matter theory to material science, quantum optics, and superconducting device fabrication.

We organize the rest of the article as follows. In Sec. II, we introduce various quasiperiodic models and Hamiltonians, and describe the theory employed for the present study. Our results for the spatial distribution of OPs, transition temperatures, and thermodynamic properties of various 1D models are discussed in Sec. III. Next, we extend our study on 1D QCs to 2D structures and investigate their properties in Sec. III. Finally, we summarize and conclude in Sec. IV.

II. MODEL AND HAMILTONIAN

We start by describing our 1D quasiperiodic model using an attractive Hubbard Hamiltonian which reads

$$\begin{aligned}
 H = & - \sum_{i,\sigma} (t_{i,i+1} c_{i,\sigma}^\dagger c_{i+1,\sigma} + \text{h.c.}) + \sum_{i,\sigma} (\epsilon - \mu) c_{i,\sigma}^\dagger c_{i,\sigma} \\
 & + U \sum_i c_{i,\uparrow}^\dagger c_{i,\uparrow} c_{i,\downarrow}^\dagger c_{i,\downarrow}
 \end{aligned} \quad (1)$$

where $c_{i,\sigma}^\dagger$ ($c_{i,\sigma}$) operator creates (annihilates) an electron of spin $\sigma = (\uparrow, \downarrow)$ at i -th site, $t_{i,i+1}$ is the nearest-neighbor hopping term which can be t_A or t_B depending upon the growth rule of the binary quasiperiodic sequences. The terms ϵ and μ are the onsite and chemical potential, respectively. U is the strength of the attractive Hubbard interaction. Throughout the present study, we consider bond models for all QCs where the hoppings are distributed following various growth rules that determine the arrangement in an aperiodic but long-range ordered fashion.

The growth of the generalized Fibonacci sequence follows a rule based on the replacements $t_A \rightarrow t_A^i t_B^j$ and $t_B \rightarrow t_A$. Now, by a proper choice of i and j , different quasiperiodic sequences are generated. The total number of bonds in $(n+1)$ -th generation is given by, $G_{n+1} = iG_n + jG_{n-1}$, with $n \geq 1$ and $G_0 = G_1 = 1$. Here we

generate 1D QC by choosing $i = j = 1$ for the Fibonacci, $i = 2, j = 1$ for the Silver-mean, and $i = 3, j = 1$ for the Bronze-mean QC, while, $i = 1, j = 2$ for the Copper-mean, and $i = 1, j = 3$ for the Nickel-mean QC [107]. Our investigation is also extended from the GFQC to other well-known quasiperiodic structures, like the Thue-Morse and period-doubling QC. The growth rules for all these QCs are shown in Table-I.

We cast our model into the Bogoliubov–de Gennes (BdG) Hamiltonian within the mean field approximation [108]. The resulting Hamiltonian is given by,

$$H_{\text{MF}} = - \sum_{i,\sigma} (t_{i,i+1} c_{i,\sigma}^\dagger c_{i+1,\sigma} + \text{h.c.}) + \sum_{i,\sigma} (\epsilon - \mu) c_{i,\sigma}^\dagger c_{i,\sigma} + \sum_i (\Delta_i c_{i\uparrow}^\dagger c_{i\downarrow}^\dagger + \Delta_i^* c_{i\downarrow} c_{i\uparrow}) \quad (2)$$

where the superconducting OP is given by $\Delta_i = -U \sum_i \langle c_{i\downarrow} c_{i\uparrow} \rangle$. The diagonalization of the mean-field Hamiltonian can be done by the Bogoliubov transformation,

$$c_{i\sigma} = \sum_n (u_{i\sigma}^n \gamma_n - \sigma v_{i\sigma}^{n*} \gamma_n^\dagger) \quad (3)$$

$$c_{i\sigma}^\dagger = \sum_n (u_{i\sigma}^{n*} \gamma_n^\dagger - \sigma v_{i\sigma}^n \gamma_n) \quad (4)$$

where the spin degree of freedom is denoted by $\sigma = \pm 1$. $\gamma_n (\gamma_n^\dagger)$ are the Bogoliubov quasiparticle annihilation (creation) operators with $u_{i\sigma}^n (v_{i\sigma}^n)$ being the electron and hole-like wavefunctions of the quasiparticles with the quantum number n . The local OP, Δ_i , must satisfy the self-consistency condition,

$$\Delta_i = -U \sum_n (u_{i\uparrow}^n v_{i\downarrow}^{n*} f(E_n) - u_{i\downarrow}^n v_{i\uparrow}^{n*} (1 - f(E_n))) \quad (5)$$

where E_n s are the positive energy eigenvalues and $f(E_n)$ is the Fermi-Dirac distribution.

We also define the average OP as

$$\langle \Delta \rangle = \frac{1}{N} \sum_i \Delta_i \quad (6)$$

where N is the total number of sites in each QC.

Our calculations are carried out using the self-consistent numerical procedure. We begin with an initial guess value of Δ_i and calculate $u_{i,\sigma}^n$ and $v_{i,\sigma}^n$ by diagonalizing the mean-field Hamiltonian of Eq. (2). Incorporating the new value of Δ_i , we self-consistently solved the Hamiltonian for various QCs.

The electronic specific heat is defined via the thermodynamic relation,

$$C_e(T) = T \frac{dS(T)}{dT} \quad (7)$$

where $S(T)$ denotes the temperature-dependent entropy of the system. The entropy takes the form [82],

$$S(T) = 2k_B \sum_n \left[\ln(1 + e^{-\beta E_n}) + \frac{\beta E_n}{e^{\beta E_n} + 1} \right] \quad (8)$$

where the summation runs over the eigenvalues E_n and $\beta = 1/(k_B T)$.

For extending our analysis to the 2D QCs, the tight-binding Hamiltonian accommodates additional hopping along the vertical directions, say, t_v between adjacent layers, in addition to the two horizontal hoppings t_A and t_B .

In our study, we use the natural unit where the Boltzmann constant $k_B = 1$ and scale U by the hopping strength, which is in the units of the energy. We do all calculations for the half-filling and set the onsite potential ϵ to zero.

III. RESULTS AND DISCUSSIONS

In this section, we present and discuss our numerical results for both 1D and 2D QCs considering various quasiperiodic orderings. Since our main results for 2D QCs qualitatively corroborate with those of 1D versions, we start with the results for 1D quasiperiodic chains for pedagogical understanding, followed by results for 2D QCs for the suitability of the mean-field calculation.

A. One-dimensional quasiperiodic chains

We start from 1D quasiperiodic chains that are constructed following various growth rules defined in Table-I. We choose five different orders from the generalized Fibonacci class (Fibonacci and two others from subclass-I and two from subclass-II) and two non-Fibonacci orders as prototype examples.

1. Generalized Fibonacci class

In this subsection, we focus on quasiperiodic chains belonging to the Generalized Fibonacci class as introduced in the previous section. While Fibonacci chains have already been studied in the literature [81–86], we include them for the sake of comparison and completeness. We consider here the bond model where the hoppings are modified following quasiperiodic sequences. In addition to the Fibonacci, we also consider two other sequences: Silver-mean and Bronze-mean, which are generated in a similar way following the growth rules mentioned in Table-I. In fact, the Silver-mean and Bronze-mean sequences are generated by increasing one of the two types (t_A) of the hoppings in the growth rule. We refer them subclass-I category, while the subclass-II family can be found by increasing the other type of hopping i.e., t_B . We illustrate the behavior of the OP and the thermodynamic properties for all these quasiperiodic chains as follows.

1.1 Behavior of OP

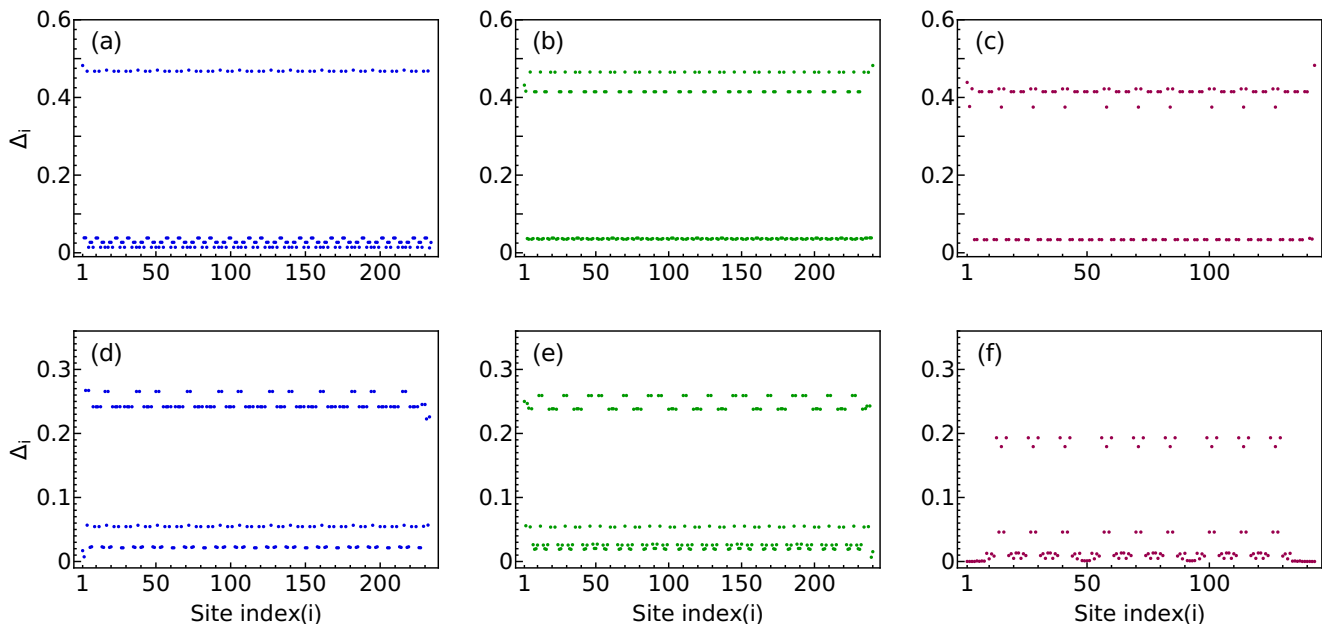


FIG. 1. Distribution of local OP in (a,d) Fibonacci, (b,e) Silver-mean, and (c,f) Bronze-mean QC for the Hubbard interaction strength $U = 1$, temperature $T = 0.01$, and the hopping amplitudes: (a-c) $t_A = 0.25$, $t_B = 1$ and (d-f) $t_A = 1$, $t_B = 0.25$.

We investigate the OP distribution across both subclasses of GFQCs for two contrasting parameter regimes: (i) $t_A < t_B$ ($t_A = 0.25, t_B = 1$) and (ii) $t_A > t_B$ ($t_A = 1, t_B = 0.25$). In both cases, the Hubbard interaction strength U ($= 1$ as mentioned in the previous section) is kept comparable to the larger of the two hopping strengths. We refer to Fig. 1 for the distribution of the local OP (Δ_i), over the lattice sites of subclass-I GFQCs. The OPs are found self-consistently using the condition mentioned in Eq. (5). We show the results of the OP for G_{12} generation Fibonacci QC consisting of 234 sites, G_7 generation Silver-mean QC with 240 sites, and G_5 Bronze-mean QC with 143 sites.¹ In periodic systems, the OP maintains a uniform (constant) value across all atomic sites because of the translational symmetry present in the lattice. However, in QCs, due to the lack of translational symmetry, the behavior of OP is position-dependent. It is sensitive to the growth rule and the choice of parameters; some atomic sites contain higher values and some are characterized by lower values of the OP, giving rise to branching of the OP. Now, the number of branches and the ratio of the OPs corresponding to the different branches depend on how the QCs are grown. We analyze it in detail to extract the underlying reason. An important point to note is that although different quasiperiodic sequences lead to entirely distinct distributions of the OP, they all exhibit a self-similar structure, a hallmark of quasiperiodicity.

In Fig. 1 (a-c), we observe that the OP profiles of the GFQC subclass-I consist of two distinct branches for

$t_A < t_B$. The lower branch has an amplitude very close to zero, whereas the upper branch contains finite OP values. Notably, in the Silver-mean and Bronze-mean QCs, this upper branch shows a slight splitting, which can be attributed to the structural frustration. This two-branching phenomenon of the OP is also true for the opposite parameter regime, that is, $t_A > t_B$ (see Fig. 1(d-f)), although the amplitude of the OP corresponding to the upper branch decreases. Comparing the OPs for all three members of the generalized Fibonacci family, we see that the Bronze-mean QC exhibits the lowest OP, indicating very low pair formation, since the total number of sites participating in the formation of the upper branch is very small compared to that in the other two QCs.

Next, we turn our attention to the GFQC subclass-II family. We consider G_8 generation Copper-mean QC and G_7 generation Nickel-mean QC, containing 172 and 218 sites, respectively. The corresponding OP profiles are shown in Fig. 2. In the Copper-mean QC, the OP amplitudes splits into three different branches: the lower branch goes to very small values, while the middle and upper branches contain different finite values for $t_A < t_B$ (see Fig. 2(a)). In contrast, the OP distribution in the Nickel-mean QC shows two branches, with a slight oscillation in the upper branch as depicted in Fig. 2(b). Interestingly, the behavior of the OP is reversed in the opposite parameter regime, i.e., $t_A > t_B$, as shown in Fig. 2(c-d). Specifically, in the Copper-mean QC, two OP branches appear, while the number of branches for the OP distributions is three for the Nickel-mean QC.

Now, the question is: what underlies the unique distribution of the OP in these quasiperiodic chains? To address this question, we conduct a detailed analysis as

¹ The generations of QCs are selected to maintain consistency in chain lengths across different structures.

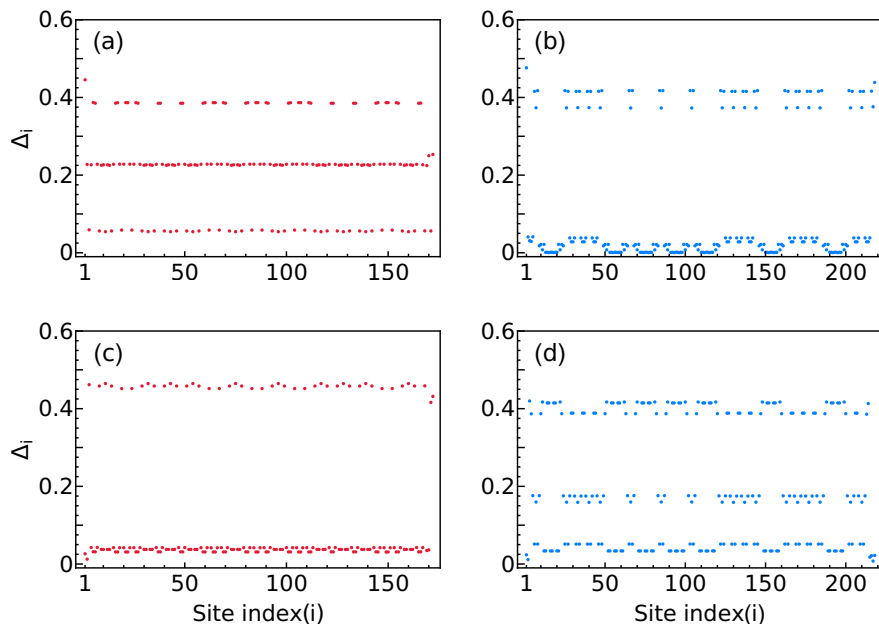


FIG. 2. Distribution of local OP over the sites of (a,c) Copper-mean and (b,d) Nickel-mean QC for (a-b) $t_A = 0.25$, $t_B = 1$ and (c-d) $t_A = 1$, $t_B = 0.25$. The rest of the parameter values are set as the same in Fig. 1.

follows. Although we consider the same onsite potential (which is zero here) for all sites throughout the chain, we identify three different kinds of sites depending on their environment set by the nearest neighbor hoppings and mark them as: α sites, which are flanked by two t_A hoppings ($t_A - t_A$), β sites surrounded by two t_B hoppings ($t_B - t_B$), and γ sites located within the environment of mixed shopping i.e., $t_A - t_B$ or $t_B - t_A$ pairs. The spatial distribution of the OP amplitudes for all five QCs is shown using color-coded markers in Fig. 3 where α , β , and γ sites under these hopping environments may or may not have same colors. Note that, in the Fibonacci, Silver-mean, and Bronze-mean QCs, the appearances of α and γ sites are permissible, while β sites are excluded by the recursive growth rules. This is true for all members of subclass-I of FGQCs. On the other hand, all three kinds of sites, α , β , γ , are present in subclass-II which includes the Copper-mean and Nickel-mean QCs of our discussions in the present work.

Let us now analyze all results shown in Figs. 1 and 2. We refer to Fig. 3 and Table-II where we summarize all our observations using color codes, at this stage for the clarity of understanding and then the following illustration. In Fig. 1 (a-c), the site-dependent OP distribution for GFQC subclass-I is shown for $t_A < t_B$. The OP amplitudes at α sites are high, indicating the higher possibility of Cooper pair formation or equivalently, lesser mobility of electrons since hopping strengths are low on either directions. Thus the electron pairs are always stuck at all α sites, and the OP at these sites can take a higher value than other sites. Due to the higher OPs at α sites than the γ sites, they are marked by two distinct colors i.e., blue and cyan color, respectively, in Fig. 3 for (a:i) Fi-

bonacci, (b:i) Silver-mean, and (c:i) Bronze-mean QC except a local fluctuation is pointed out by the green color. The description of the OP behavior is verified when we investigate the opposite parameter regime.

For the reverse parameter regime, i.e., $t_A > t_B$, OP amplitudes are the lowest in magnitude at all α sites of the Fibonacci and Silver-mean QCs, in contrast to the previous parameter regime (see Fig. 3(a:ii) and (b:ii)). The electrons are likely to hop from all α sites (marked by cyan color) to their neighboring γ sites, instead of pair formation. However, all γ sites are not at the same standard from the pair formation point of view. They may or may not possess higher OP. All γ sites which are only within γ - α - γ environments show higher OP amplitudes. Thus, γ sites are colored using both cyan (for lower OP) and magenta (for higher OP) colors. These phenomena are true for both Fibonacci and Silver-mean QCs. Note again that, we use different colors to highlight various ranges of OP amplitudes irrespective of the sites. It turns out that any particular type of sites for a particular QC may or may not be marked by the same color. It depends on the quasiperiodicity as well as the hopping ratio. Interestingly, in the Silver-mean QC, there can appear another type of cluster: γ - α - γ in addition to the γ - α - γ cluster which can affect the behavior of the OP. Among these structural units, the pairing probability is high at γ sites of the γ - α - γ cluster, leading to higher OP values. In contrast, the γ sites exhibit reduced OP while sitting within γ - α - α - γ cluster (see Fig. 3 (b:ii)). In the Bronze-mean QC, γ - α - α - γ and γ - α - α - α - γ are only allowed clusters to appear; the γ - α - γ cluster never appears. These structural constraints lead to an overall lower OP profile in the Bronze-mean QCs. Within the

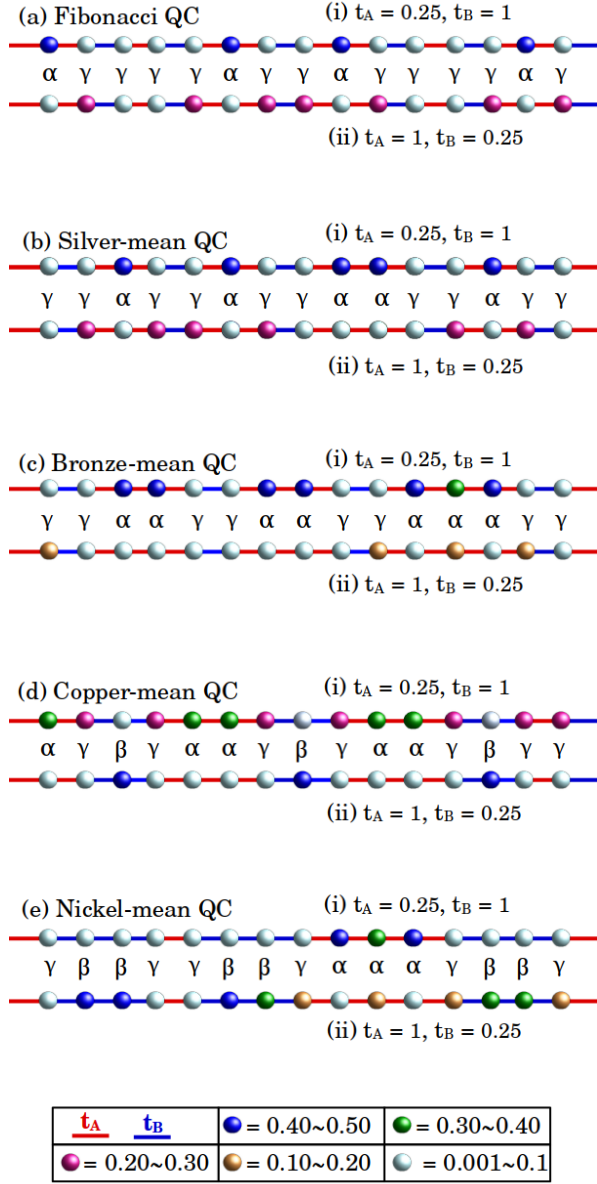


FIG. 3. Color-coding of various sites α , β , and γ , according to the distribution of OP across sites of GFQCs for the two parameter regimes. The rest of the parameter values are kept the same as in Fig. 1.

γ - α - α - α - γ cluster, the middle α sites and the two outer γ sites can have lower but finite amplitudes of the OP (see Fig. 3 (c:ii)). The corresponding plots of OP profiles are demonstrated in Fig. 1 (d-f) for the subclass-I of GFQCs. For the clarity of the comparison, we denote the site types in each figure and also show the comparison based on OP amplitudes in Table-II.

Now, we move on to the subclass-II of GFQC family. The key difference between the two subclasses of GFQC is that subclass-II QCs can host all three kinds of sites, α , β , and γ as defined previously. For the parameter regime $t_A < t_B$, the behaviors of the OPs for subclass-II

TABLE II. List of OP amplitudes in GFQCs with colors mentioned the same as shown in Fig. 3.

Parameter regime	QCs	higher OP (color)	lower OP (color)
$t_A = 0.25$ $t_B = 1$	Fibonacci	all α (blue)	all γ (cyan)
	Silver-mean	all α (blue)	all γ (cyan)
	Bronze-mean	all α (blue)	all γ (cyan)
$t_A = 1$ $t_B = 0.25$	Fibonacci	γ (magenta) in γ - α - γ	all α (cyan) other γ (cyan)
	Silver-mean	γ (magenta) in γ - α - γ	all α (cyan) other γ (cyan)
	Bronze-mean	γ (yellow) and middle α (yellow) in γ - α - α - α - γ	other α (cyan) other γ (cyan)
$t_A = 0.25$ $t_B = 1$	Copper-mean	all α (green) γ (magenta) in γ - β - γ	all β (cyan) other γ (cyan)
	Nickel-mean	all α (blue)	all β (cyan) all γ (cyan)
$t_A = 1$ $t_B = 0.25$	Copper-mean	all β (blue)	all α (cyan) all γ (cyan)
	Nickel-mean	all β (blue) γ (yellow) and middle α (yellow) in γ - α - α - α - γ	other α (cyan) other γ (cyan)

GFQCs are quite similar to those of subclass-I GFQC family in spite of the appearance of three distinct lattice sites. Relatively higher OP appears at all α sites, while OPs at β sites are vanishingly small as shown in Fig. 3 (d:i) for Copper-mean and (e:i) for Nickel-mean QC. As $t_A < t_B$, electrons that participate in Cooper pair formation have a higher chance to move to neighbouring γ sites of γ - β - γ cluster. As a consequence, two γ sites in γ - β - γ cluster can take a finite value of OP as seen in the Copper-mean QC (but still, it is lower compared to the α site). In Fig 2 (a,b), the corresponding OP distributions are shown for the Copper-mean and Nickel-mean QC, respectively. For the Copper-mean QC, the non-zero part of the OP breaks into two branches: the higher at α sites, lower at γ sites of the γ - β - γ cluster.

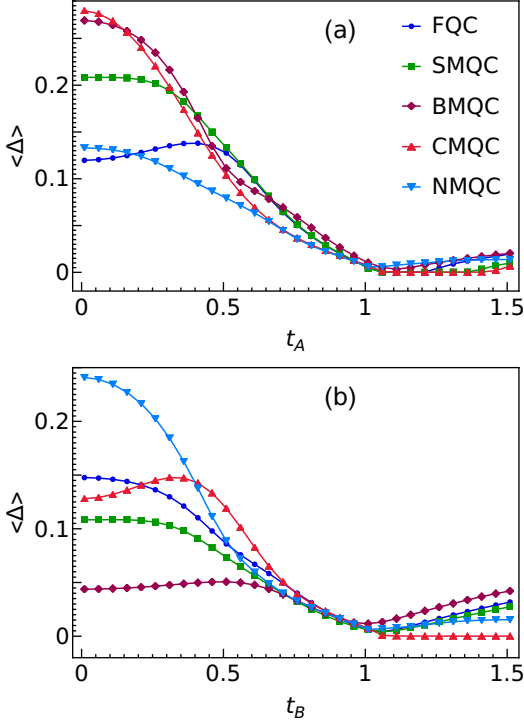


FIG. 4. Behavior of average OP as a function of hopping strength (a) t_A keeping $t_B = 1$ and (b) t_B with t_A for generalized Fibonacci class members. The rest of the parameter values are maintained as in Fig. 1. The abbreviations are as follows: FQC: Fibonacci QC, SMQC: Silver-mean QC, BMQC: Bronze-mean QC, CMQC: Copper-mean QC, and NMQC: Nickel-mean QC.

Interestingly, the OP distribution undergoes a noticeable change when we reverse the hopping parameters across the QCs. For $t_A > t_B$, the β sites contain higher OP in the Copper-mean and Nickel-mean QC as shown in Fig. 3 (d:ii) and (e:ii), respectively. In the Nickel-mean QC, the middle α and outer γ sites of γ - α - α - γ clusters can take a lower OP amplitudes similar to the Bronze-mean QC (see Fig. 3(e:ii)). The corresponding OP profiles for Copper-mean QC and Nickel-mean QC are demonstrated in Fig. 2 (c-d). For the same parameter regime, the non-zero OP profile of Nickel-mean QCs has two branches, the higher one due to β sites and the lower one for the middle α and outer γ sites of γ - α - α - γ clusters. We again refer to Fig. 3 and Table-III for the summary. We present all discussions on the spatial distribution of the OP for a particular Hubbard interaction U , fixed at the value of the higher hopping amplitude, although the behaviors of OP will remain qualitatively similar for low to moderate U , but not for strong U .

So far, the behavior of the OP has been studied for two parameter regimes. In order to understand the evolution of the OP across the whole range of the hopping ratio more clearly, we plot the average OP defined in Eq. (6) as a function of t_A (t_B) in Fig. 4(a) (Fig. 4(b)), keeping the other one fixed at unity i.e., $t_B = 1$ ($t_A = 1$). Note that,

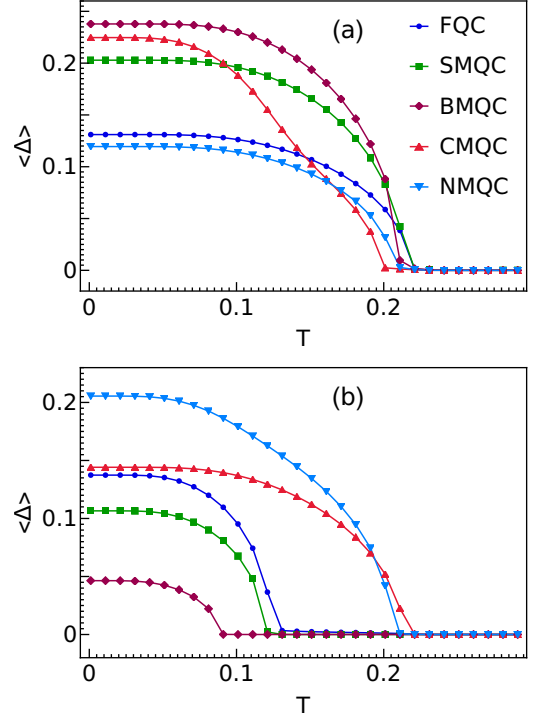


FIG. 5. Variation of average OP with temperature for the GFQCs for different choices of hopping amplitudes (a) $t_A = 0.25, t_B = 1$, (b) $t_A = 1, t_B = 0.25$. The rest of the parameter values are maintained as in Fig. 1 and the abbreviations are the same as in Fig. 4.

both these figures can reveal the behavior of the OP for both parameter regimes i.e, $t_A < t_B = U$ and $t_A = U > t_B$ as discussed previously. However, we always had $U = 1$. We did not arrive at the situation when $t_A > U > t_B$ or $t_B > t_A > U$. It matters whether the Hubbard interaction strength is comparable to t_A or t_B , although it is kept fixed to 1. The effect of the ratio of the Hubbard strength to the hopping will be clear from the following analysis.

By comparing all QCs in Fig. 4(a), we find that the Fibonacci and Nickel-mean QCs show lower average OP while, the Bronze mean and Copper-mean exhibit the higher values among all these five GFQCs for $t_A < t_B = U$. These have already been discussed previously. Now, on further tuning the hopping parameter, t_A reaches the value of t_B , i.e., $t_A = t_B = 1$, which describes the simple regular 1D periodic chain, and all OP curves converge to a single point. Further increment of t_A not only reaches the contrast parameter regime ($t_A > U > t_B$) but also makes t_A higher than U , which eventually leads to suppressed pair formation with much lower average OP. In Fig. 4(b), as we tune t_B maintaining $t_A = U > t_B$, the Nickel-mean QC exhibits the highest average OP as a large number of β sites appear here. However, in the Bronze-mean QC, the formation of β or γ - α - γ cluster is never possible. As a consequence, the average OP of Bronze-mean QC is very small compared to other QCs. Other features can also be described using similar jus-

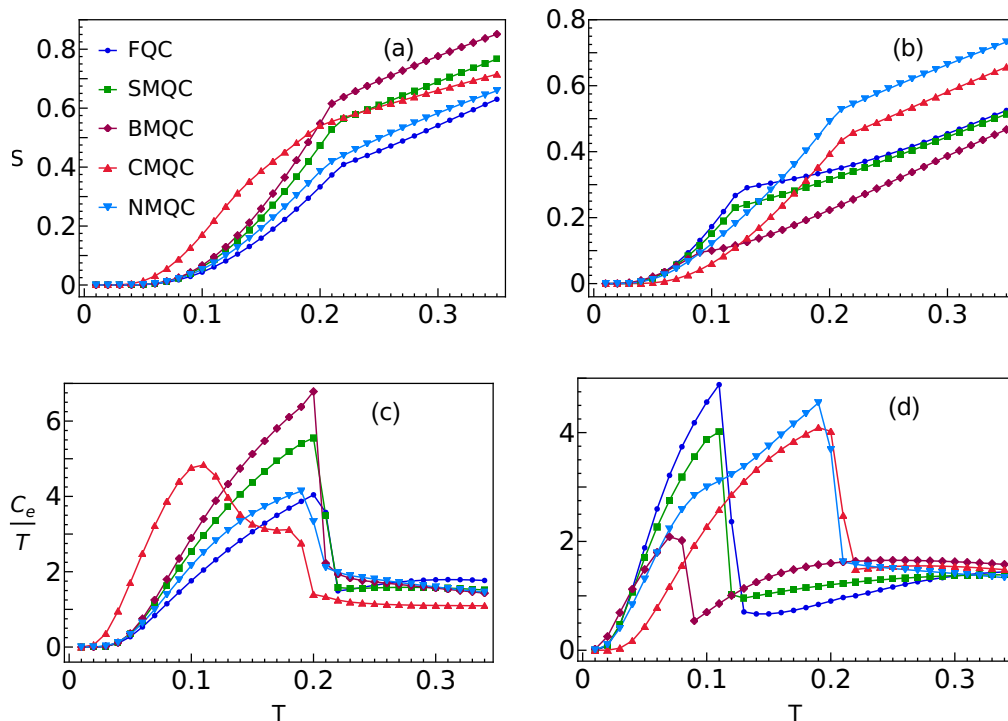


FIG. 6. (a,b) Entropy and (c,d) electronic specific heat vs. temperature for the GFQCs with (a,c) $t_A = 0.25$, $t_B = 1$ and (b,d) $t_A = 1$, $t_B = 0.25$. The rest of the parameter values are maintained as in Fig. 1 and the abbreviations are the same as in Fig. 4.

tifications mentioned in the previous paragraph. Most importantly, when $t_B > U > t_A$, all OPs are suppressed and quite similar in their behavior.

Now, an interesting and important question is: how does the OP change with temperature? In periodic systems, the OP typically shows a smooth and well-understood decreasing behavior with increasing temperature and eventually vanishes at a well-defined critical temperature T_c . This critical point marks a phase transition beyond which the system loses its pair formation phase, and the average OP drops to zero. However, in QCs, the lack of translational symmetry and the variation in the local environment can affect the variation of the OP as well as the critical temperature. To explore this, we calculate the average OP with the variation in the temperature. Fig. 5(a) corresponds to the parameter regime $t_A < t_B$, which encodes higher OP values at α sites. For the GFQC subclass-I family, the number of α sites is maximum for the Bronze-mean QC and minimum for the Fibonacci QC. Due to this, the average OP values at low temperature regime follow the order: Bronze-mean, Silver-mean, and Fibonacci QC in the increasing order. For subclass-II, in the Nickel-mean QC, the number of α sites is small compared to β or γ sites. Whereas the Copper-mean QC has almost the same number of α and β sites, and additionally the γ sites of γ - β - γ contain a finite OP value. So, in the GFQC subclass-II family, the average OP in the lower temperature regime is the highest for the Copper-mean QC and lowest for the Nickel-mean QC. Overall, within the GFQC family,

the Bronze-mean and Copper-mean QC are more prone to the Cooper pair formation. In this case, the transition temperatures T_c converge to nearly the same values. However, the rate of change of the OP for the Copper-mean QC is higher than that in the Bronze-mean QC.

For the reverse situation ($t_A > t_B$), the β site contains maximum values of the OP as shown in Fig. 5(b). Now, in the GFQC subclass-I family, there is no β site. Here, mainly the finite OP is hosted by γ sites of the γ - α - γ clusters (for the Fibonacci and Silver-mean QC). The appearance of the γ - α - γ clusters in the Fibonacci QC is more frequent than in the Silver-mean QC, whereas this type of cluster never appears in the Bronze-mean QCs. Here, γ and the middle α sites of γ - α - α - γ clusters can contain the lower OP. Additionally, the appearance of this cluster is rare throughout the structure. As a result, the average OP and their transition temperatures T_c follow the order: Fibonacci, Silver-mean, and Bronze-mean QC in the increasing order in the magnitude, for the GFQC subclass-I family as shown in Fig 5(b). For the subclass-II, both the Copper-mean and Nickel-mean QC contain β sites. As the Nickel-mean QC contains a large number of β sites, its average OP exhibits a higher magnitude than the Copper-mean QC at the low temperature regime. So, under this environment within the whole generalized Fibonacci family, the Nickel-mean (Bronze-mean) QC has the highest (lowest) average OP in the low temperature regime. Moreover, the corresponding transition temperatures appear at distinct values (see Fig.-5(b)). Note that,

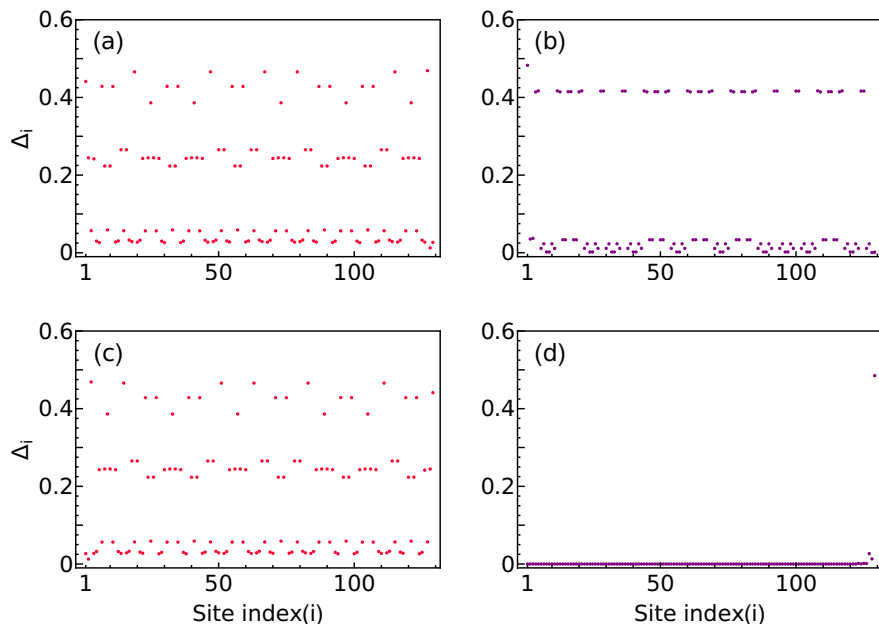


FIG. 7. Local OP amplitudes at various sites in 1D (a,c) Thue-Morse and (b,d) Period-doubling QC. The hopping terms are chosen as: (a,b) $t_A = 0.25, t_B = 1$, (c,d) $t_A = 1, t_B = 0.25$. The rest of the parameter values are set as the same in Fig. 1.

the transition temperatures vary widely for the QCs in the latter parameter regime.

It is clear that the variation of the average OP with temperature is not universal across different quasiperiodic sequences. Instead, it shows distinct behaviors depending on the underlying growth rule and the specific choice of model parameters. Also, the behavior of the OP is not random; they are explainable by the underlying arrangement of the QCs.

For each QC, the temperature dependence of the superconducting OP is shaped by the spatial modulation of the local environment, which directly influences the pairing amplitude at each site. By analyzing how the OP changes, one can accurately determine the transition temperature for different QCs. Comparison of the transition temperatures across various QCs reveals which configurations enhance or suppress the possibility of superconductivity. This understanding is not only fundamental for characterizing possible superconducting phases in such complex systems, but also lays the groundwork for future research aimed at a better understanding of the QC-based superconductivity. In all the OP calculations throughout the present work, the Hartree shift term is not taken into account unless mentioned. Note that, the distribution of the OP will be significantly affected by the Hartree-shift term in the strong interaction regime. The effect of the Hartree shift on OP in the parameter regime we consider is discussed in Appendix A.²

1.2 Thermodynamic properties

We now focus on the thermodynamic behavior of these QCs in terms of the entropy and electronic specific heat, which serves as a sensitive probe of the quasiparticle excitation spectrum and provides information about the possible superconducting phases. The behaviors of entropy $S(T)$ and electronic specific heat $C_e(T)/T$ with temperature are shown in Fig. 6 for GFQCs, considering the two parameter regimes. At low temperatures, the state is highly ordered, with most electrons forming Cooper pairs, resulting in lower entropy. As temperature increases, thermal excitations break pairs resulting in increasing disorder and entropy. The electronic specific heat profiles drop sharply at the transition temperatures for most of the QCs. This sudden change is a clear sign of the phase transition. Above the transition temperature, the specific heat behaves more smoothly.

However, there are some changes found in the behavior of both the entropy and specific heat when we switch the parameter regimes. Specifically, for $t_A < t_B$, all members of the generalized Fibonacci family show a similar pattern for the temperature dependence except the Copper-mean QC (see Fig. 6(a,c)). The reason behind this unique thermodynamic behavior of the Copper-mean QC is hidden in its OP distribution, or equivalently, the structural growth. As discussed earlier, the non-zero OP profile of the Copper-mean QC breaks into two parts: the higher one is for α sites, and the other is for the γ sites of the γ - β - γ cluster (see Fig. 2 (a)). Now, as the temperature

² Note that, we do not confirm the superconductivity in the present work. We only confirm the possibility of pair formation. Super-

conductivity can be confirmed by further investigation on the superconducting coherence, which we plan to report in future work.

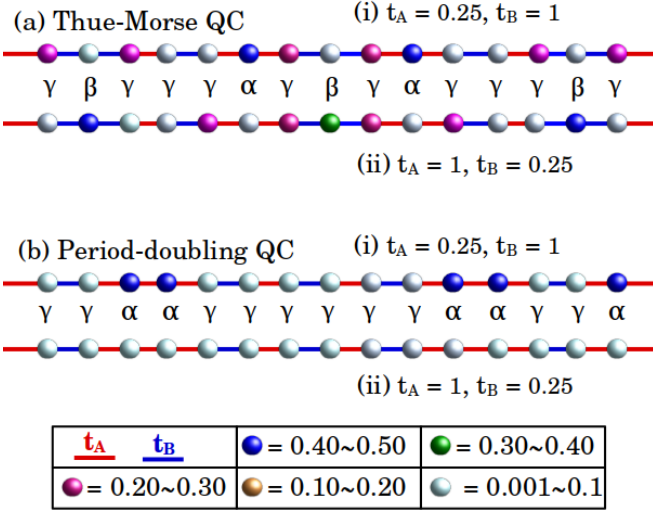


FIG. 8. Color-coded distribution of OP amplitudes in (a) Thue-Morse and (b) Period-doubling QC. The rest of the parameter values are set as the same in Fig. 1.

rises, the OP magnitudes of both branches decrease, and the lower branch goes to zero, whereas the higher branch still contains non-zero values. It approaches zero with further increasing temperature. Due to this, the entropy and electronic specific heat for the Copper-mean QC vary in an unusual way. The first decay of C_e from the peak is due to the suppression of OP values at γ sites of γ - β - γ cluster, the second and final fall indicates the disappearance of the OP at α (and also from γ) sites (see Fig. 6(c)). Following the same reason, the rapid fall of the average OP with temperature for Copper-mean QC (see Fig. 5(a)) can be explained.

For the contrast parameter regime, the behaviors of the entropy and the specific heat for the generalized Fibonacci QC family are shown in Fig. 6(b,d). Interestingly, the profiles show phase transition at different T_c , which corroborate our findings mentioned in the previous subsection. Note that, the behavior of the specific heat profile for the Nickel-mean QC shows different behavior from that in the other QCs. It is characterized by a small curvature, which can be explained in the following way. Among the two non-zero OP branches of the Nickel-mean QC, the lower branch goes down to zero rapidly, followed by the decreasing behavior of the other branch. This two-step process is reflected in the curvature profile (see Fig. 6(d)).

2. QCs from non-Fibonacci class

To enhance the depth and completeness of our work, we now extend our investigation beyond the Fibonacci QC. By exploring other aperiodic structures, each with distinct geometric and spectral features, we aim to show

TABLE III. OP distribution over different sites of non-Fibonacci QCs.

Parameter regime	QCs	higher OP (color)	lower OP (color)
$t_A = 0.25, t_B = 1$	Thue-Morse	all α (blue) γ (magenta) in γ - β - γ	all β (cyan) other γ (cyan)
	Period-doubling	all α (blue)	all γ (cyan)
$t_A = 1, t_B = 0.25$	Thue-Morse	all β (blue) γ (magenta) in γ - α - γ	all α (cyan) other γ (cyan)
	Period-doubling	—	all α (cyan) all γ (cyan)

that our way of analysis is not only valid for the Fibonacci, but it is also valid for the non-Fibonacci class. To minimize repetitions of analysis, we only choose two QCs from the non-Fibonacci family: Thue-Morse and Period-doubling QC, and explain only the behaviors of the OP in the main text, since other behaviors will follow this description. Note that, the growth rules for these two sequences are already mentioned in Table I. We consider both these QCs in their G_8 -th generation, containing 129 sites.

2.1 Behavior of OP

Fig. 7 shows the variation of the local OP over sites for the Thue-Morse and period-doubling QC. In the Thue-Morse QC, all three α , β , and γ site appear similar to the subclass-II of GFQC. When $t_A < t_B$, all α sites exhibit higher OP values (see Fig. 8 (a:i)). On the other hand, the OP amplitudes at β sites are suppressed due to the higher hopping probability to their neighbor γ sites. Hence, these γ sites of γ - β - γ cluster exhibit a finite OP (low compared to α sites). The OP profiles for these QCs are depicted in Fig. 7(a), showing two finite OP branches for α sites and for γ sites within the γ - β - γ clusters.

For the reverse situation $t_A > t_B$, the distribution of the OP is completely reversed. Now α sites contain the lowest OP amplitude, whereas the OP amplitudes at the β sites are higher, unlike GFQCs. Additionally, the γ sites exhibit a finite OP (lower compared to β sites), which comes from γ - α - γ cluster, not from γ - β - γ cluster (see Fig. 7(c)). We present this by color-coding in Fig. 8(a:ii).

For the period-doubling QC, the formation of the β site is never possible as found in the GFQC subclass-I family. At $t_A < t_B$, only α sites have the higher OP amplitudes as shown in Fig. 7(b) and Fig. 8(b:i). When the period-doubling QC is subjected to the reverse parameter regime, i.e., $t_A > t_B$, the OP at all sites becomes

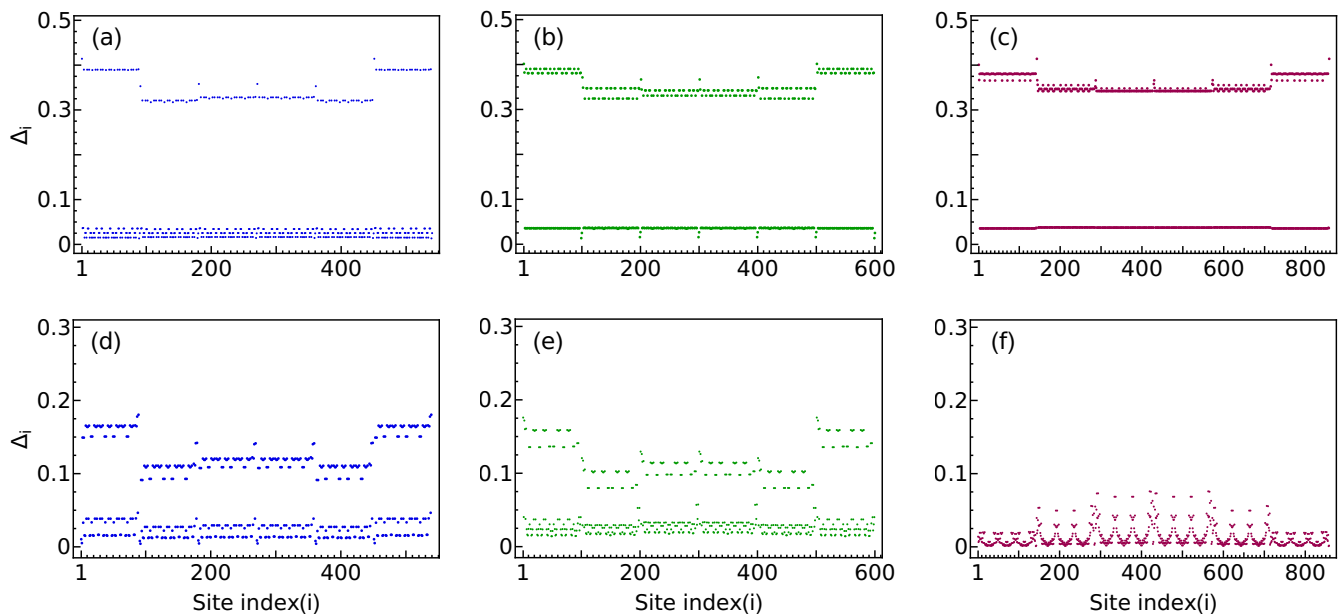


FIG. 9. Distribution of OP over sites for 2D (a,d) Fibonacci, (b,e) Silver-mean QC, (c,f) Bronze-mean QC for $t_v = 0.25$ and (a-c) $t_A = 0.25$, $t_B = 1$ and (d-f) $t_A = 1$, $t_B = 0.25$. Other parameters are the same as in Fig. 1.

very close to zero. Due to the formation of the β sites, as well as γ - α - γ (present in the Fibonacci and Silver-mean QC too) or γ - α - α - α - γ (present in Bronze-mean and Nickel-mean QC too) cluster is never possible here. The OP profile and the corresponding schematic diagram for the period-doubling QC are depicted in Fig. 7(d) and Fig. 8(b:ii), respectively. We denote the site types and show the OP amplitudes comparison in Table-III. We find that the behavior of the average OP with temperature and thermodynamic behaviors for these non-Fibonacci QCs are close to the GFQCs, which we explicitly present in Appendix B.

B. 2D QCs

Finally, we extend our investigation to 2D QCs keeping in mind the validation of the mean-field analysis and present our results for the OP in Fig. 9. We construct the 2D lattices by vertically stacking M number of 1D quasiperiodic chains as shown in Fig. 10. Unlike 1D QCs, where only two types of overlap integrals appear for all growth rules we consider, the 2D structure allows increased complexity in the local bonding environments due to the additional hopping. Specifically, three distinct types of overlap integrals can appear, denoted by t_A , t_B , and t_v , each of them corresponding to different geometric arrangements of neighboring sites. Interestingly, our analysis in the 2D setting not only aligns with but also reinforces our key findings obtained from the 1D case, highlighting the robustness of the observed physical behaviors of OP distributions across different dimensions. We consider 2D G_{10} -th Fibonacci QC containing 540

sites, G_6 -th generation Silver-mean QC with 600 sites, and G_5 -th generation Bronze-mean QC consisting of 858 sites for the two different parameter regimes. Figure 9 illustrates the spatial distribution of the OP across the 2D GFQCs. We observe that the OP profiles are more enriched than the 1D counterpart. The OP distributions of 2D GFQC subclass-II and non-Fibonacci families are elaborately discussed in Appendix C.

For $t_A < t_B$, the superconducting OP profiles of the 2D GFQC subclass-I members exhibit two primary branches similar to those found 1D systems, see Fig. 9(a-c). Conversely, at the reverse parameter regime, i.e., $t_A > t_B$, the overall OP of the GFQC subclass-I appears at smaller amplitudes compared to the previous regime. These OP profiles are depicted in Fig. 9(d-f). While the overall qualitative behavior is preserved, quantitative differences arise in the OP amplitudes. This happens mostly due to the differences in the generation number between the 1D and 2D QCs. Due to computational resource limitations, we consider lower-generation QCs in the 2D case compared to the 1D counterpart, resulting in a smaller number of lattice sites along the horizontal direction with quasiperiodic sequences, although the total number of sites in the 2D systems is large. It is worth noting that edge effects are present in all OP profiles. Such effects have been previously discussed in the literature [94, 97, 109–112]. We confirm that the influence of edge effects decreases as the generation number increases, leading to more uniform bulk behavior in higher-generation lattices.

However, the basic patterns of the OP profiles in the 2D systems are very similar to those in 1D. The corresponding schematic diagram of 2D QCs at the parameter

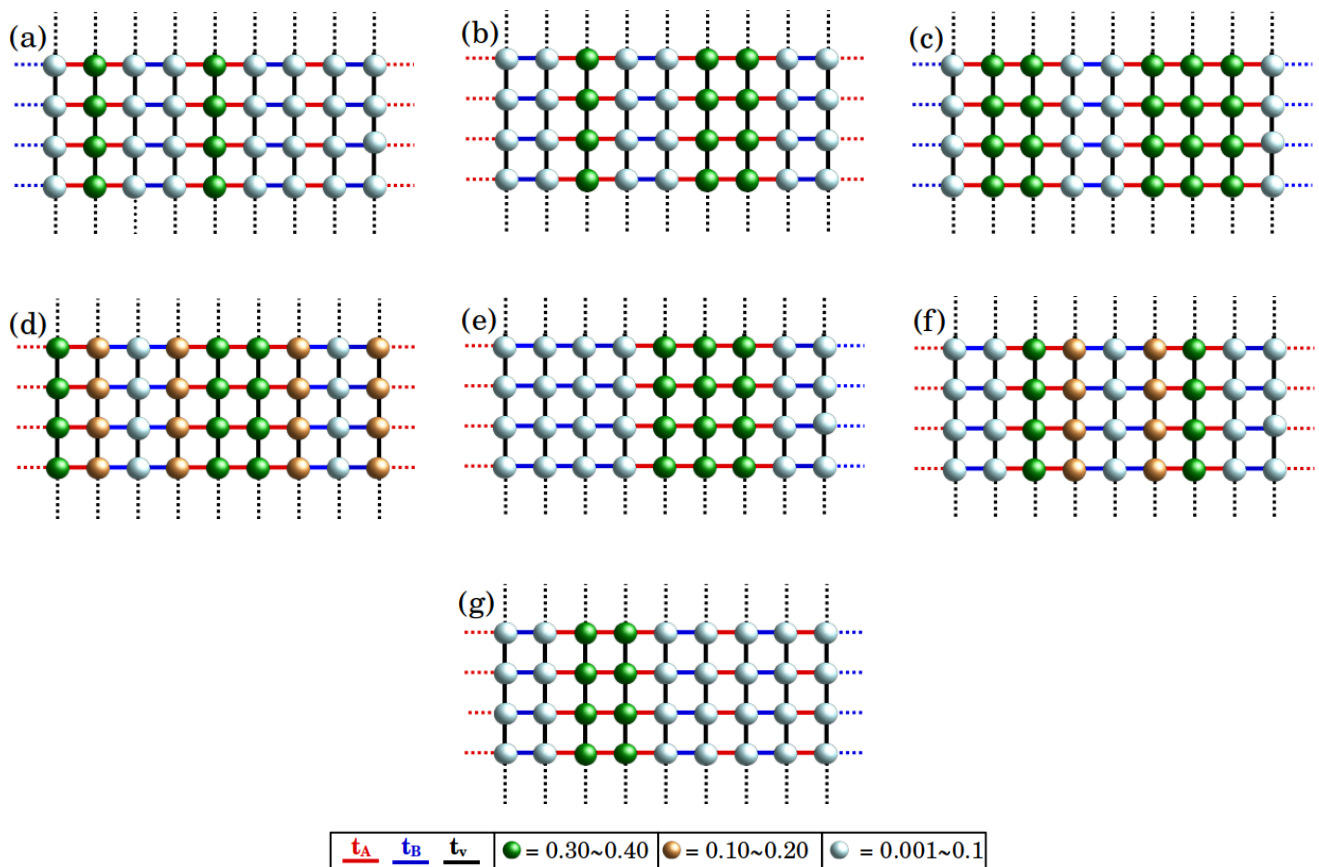


FIG. 10. Behavior of OP in 2D (a) Fibonacci, (b) Silver-mean, (c) Bronze-mean, (d) Copper-mean, (e) Nickel-mean, (f) Thue-Morse, and (g) Period-doubling QC with the local OP distribution marked by using color code. The horizontal hopping is t_A or t_B depending on the growth rule, whereas along the vertical, the hopping term is t_v . The parameters are chosen as $t_A = 0.25, t_B = 1, t_v = 0.25$. The rest of the parameter values are set as the same in Fig. 1.

regime $t_A < t_B$ is shown in Fig. 10 for both the GFQC and non-GFQC. We consider the vertical hopping term t_v equal to the lower hopping. As discussed in 1D case, here also the α sites contain the highest magnitude of OP. The corresponding sites are marked by green color as shown in Fig. 10(a-g) for 2D Fibonacci, Silver-mean, Bronze-mean, Copper-mean, Nickel-mean, Thue-Morse, and Period-doubling QCs respectively. Additionally, as seen in 1D case, here also the γ sites in $\gamma - \beta - \gamma$ exhibit finite OP amplitudes. It is also true for 2D Copper-mean and Thue-Morse QCs as demonstrated in Fig. 10(d) and (f), by yellow color.

A natural question appears at this point: does the vertical hopping t_v affect the OP distribution across the QCs? The answer is yes, it does. Here, we show all results for t_v to be equal to either t_A or t_B . However, when t_v is very small compared to t_A or t_B , electron hoppings along the vertical direction will become more restricted. This reduced mobility enhances electron localization, which in turn facilitates the formation of Cooper pairs. As a result, the superconducting OP increases in magnitude. We also discuss the effect of the vertical hopping on the OP in Appendix C. On the other hand, if t_v is increased

beyond t_A or t_B , electrons can move more freely in the vertical direction. This higher mobility tends to spread out the electrons, making it difficult for the pair formation. As a result, the superconducting OP decreases. In the extreme case where t_v competes with $t_{A(B)}$ and U , the OP is suppressed across the entire QC and can become nearly zero at all sites, indicating that the pair formation phase is lost. This consistency across the dimensions suggests the universality of the underlying physical behavior to some extent, regardless of the dimensional extension of the QC structure. The behavior of the average OPs with the temperature for the GFQCs are demonstrated in Appendix C. The behaviors of the curves for all GFQCs are almost the same as discussed for 1D cases, only with a marginal difference in the magnitudes.

IV. SUMMARY AND CONCLUSIONS

In summary, we have carried out a comprehensive investigation on the emergence and behavior of the superconducting OP in a broad class of 1D QCs, and further extended our analysis to 2D systems. We have focused on

the spatial structure of the OP, its sensitivity to system parameters, and their thermal responses. Using a self-consistency framework, we have investigated how the superconducting OP behaves across QCs, identifying which sites support enhanced OP and which sites suppress it. This spatially resolved analysis has revealed that pair formation in QCs is strongly influenced by the local structural motifs that arise from their underlying quasiperiodic order. Our analysis has demonstrated that both the nearest-neighbor hopping amplitude and the strength of the attractive on-site Hubbard interaction are crucial for the behavior of the OP. The competition between different kinds of sites or clusters underlying quasiperiodic geometry gives rise to a rich and nontrivial OP landscape that deviates significantly from the conventional periodic lattices.

We have also explored the temperature dependence of the OP in QCs for various parameter regimes. We have found that the transition temperatures vary significantly across the collection of QCs and thus are not universal. It was found to vary significantly depending on both the model parameters and the specific quasiperiodic sequence. By systematically comparing the parameter regimes, we identify optimal combinations of hopping and interaction strengths that are favorable for achieving higher OP across the QC family. Conversely, we have also pointed out the parameter regimes where the OP is significantly weakened.

Finally, we have examined the thermodynamic properties of QCs in terms of the entropy and electronic specific heat, which show distinct variations depending on the specific choice of the quasiperiodic sequence and the associated model parameters. The behaviors of these thermodynamic quantities in QCs are consistent with the behaviors of the OP, further reinforcing our main findings.

From the experimental perspectives, these QCs have been shown to be synthesized by the electron or single-beam holography [113–115]. Various QCs and their approximants have also been experimentally realized by proper choice of compound materials, like Al-Mg-Zn, Al-Cu-Li, Mg-Ga-Al-Zn alloys [116–119]. The superconducting phases in the Fibonacci QC and its approximants have been uncovered in Al-Zn-Mg alloy [80]. This provides a way for the experimental realizations in a broader range of aperiodic systems for both 1D and 2D systems including Penrose and Moire patterns in twisted materials [120–127].

Our findings not only enrich the theoretical understanding of the pair formation in a broad range of QCs, but also offer valuable guidance for the experimental realization since this approach will help in determining the most promising structure for realizing the pair formation phase. These results may also serve as a useful theoretical foundation for interpreting calorimetric measurements in engineered QCs. Note that, in the present study, we do not confirm any superconductivity. It needs further investigations which we plan for the future study.

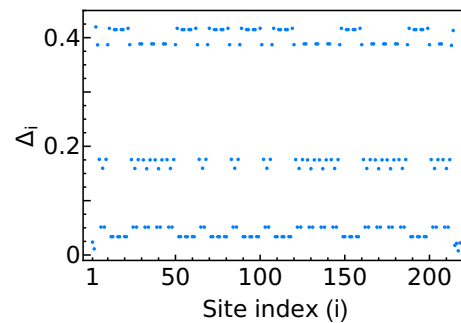


FIG. 11. OP profile of 1D Nickel-mean QC, when Hartree shift term is taken into account. The parameters are chosen as $t_A = 1$, $t_B = 0.25$. The rest of the parameter values are set as the same in Fig. 1.

V. ACKNOWLEDGEMENT

We acknowledge the Department of Space (DoS), Government of India, for all support at Physical Research Laboratory (PRL) and also the ParamVikram-1000 HPC facility at PRL, Ahmedabad, for carrying out a major part of the calculations. S.B. thanks Kuntal Bhattacharyya for some helpful discussions. P.D. thanks Anica Black-Schaffer, B. Andrei Bernevig, and Adolfo G. Grushin for constructive comments and suggestions, and Debmalya Chakraborty for some helpful discussions. We thank Miguel Ángel Sánchez-Martínez for careful reading of the manuscript and valuable comments.

Appendix A: Effect of Hartree shift

Throughout the present study, all the results are shown without considering the Hartree shift term. In this subsection, we show the effect of the Hartree shift term with which the effective onsite potential part of the Hamiltonian becomes, $\epsilon_{eff} = \sum_{i,\sigma} (\epsilon + \epsilon_i^{HF} - \mu) c_{i,\sigma}^\dagger c_{i,\sigma}$. The chemical potential μ can be determined by the average electron filling [95]:

$$\langle n_e \rangle = \frac{1}{N} \sum_i n_e(i) \quad (\text{A1})$$

where,

$$n_e(i) = 2 \sum_n [|u_i^n|^2 f(E_n) + |v_i^n|^2 (1 - f(E_n))]. \quad (\text{A2})$$

At the half filling, $\langle n_e \rangle = 1$. The self-consistency equation for the Hartree shift becomes: $\epsilon_i^{HF} = -\frac{U}{2} n_e(i)$ [94]. Now, to calculate the OP self-consistently, we begin with an initial guess value of μ , Δ_i , and ϵ_i^{HF} , and then calculate $n_e(i)$ with the new Δ_i and ϵ_i^{HF} using the quasiparticle energies and wavefunctions. This step is repeated until the convergence is achieved [128]. We adjust μ in such a way that the system is always in its half-filling condition. We find that after considering the Hartree shift

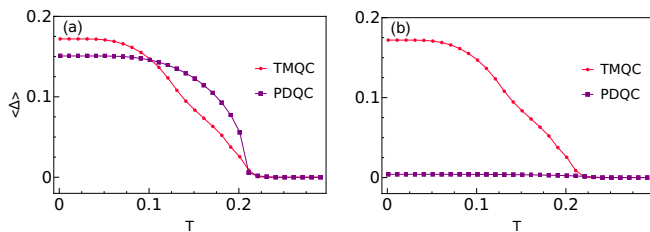


FIG. 12. Behaviour of the average OP with temperature for Thue-Morse (TMQC) and Period-doubling QC (PDQC) with (a) $t_A = 0.25$, $t_B = 1$ and (b) $t_A = 1$, $t_B = 0.25$. The rest of the parameter values are maintained as in Fig. 1.

term, there is a nominal change in the behavior of the OP as long as the Hubbard interaction is not strong. Specifically, the overall nature of the OP distribution and its magnitudes remain almost unaffected when the Hartree shift term is taken into account. In order to show the effect of the Hartree term, we show the behavior of the OP only for the Nickel-mean QC in Fig. 11 as an example. Compared with Fig. 2, we observe that the OP profiles with and without the Hartree term are very similar to each other. We also confirm the same for other QCs. Thus, the non-consideration of the Hartree-shift term is completely justified as long as the interaction is not strong, since the qualitative behavior remains unaffected, making nominal changes in the amplitudes.

Appendix B: A few more results for non-Fibonacci 1D QCs

In this section, we present the temperature dependence of the average OP for two 1D non-Fibonacci QCs: Thue-Morse and period-doubling QCs in Fig. 12. When we choose the parameter regime $t_A < t_B$ (see Fig. 12(a)), behavior of the OP is very similar to that for the GFQC. Both these QCs contain the α sites that cause a higher value of the OP. Additionally, the Thue-Morse QC has a finite OP at the γ sites of γ - β - γ cluster. Due to this, at the low temperature regime, the average OP of the Thue-Morse QC is slightly higher than the Period-doubling QC. As the temperature increases to a higher value, the overall OP profile decreases and goes to zero at the transition temperature similar to the GFQC.

Conversely, when we choose the opposite parameter regime as $t_A > t_B$, β and γ sites (in γ - α - γ cluster) play the main role to contain the higher OP values. As both structural units are present in the Thue-Morse QC, it has a high average OP at low temperature regime and also has a finite transition temperature as shown in Fig. 12(b). On the other hand, in the period-doubling QC, the amplitude of OP goes to zero due to the absence of any β site or γ - α - γ cluster at any finite temperature. Here also, the average OP in the Thue-Morse QC falls rapidly with temperature. This happens due to the branching behavior of the non-zero OP profile, similar to the Copper-mean QC

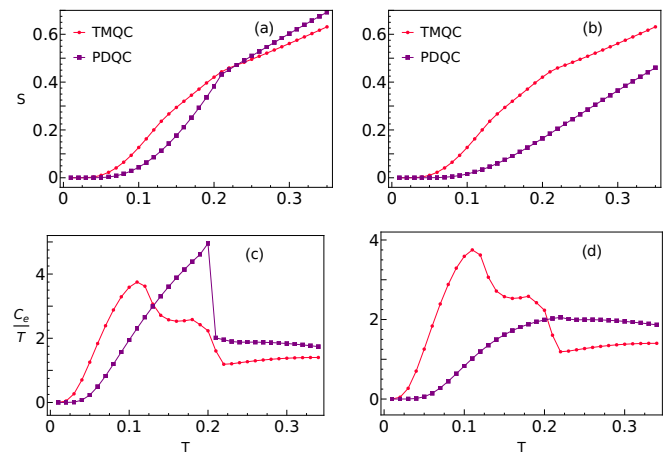


FIG. 13. (a,b) Entropy and (c,d) electronic specific heat as a function of temperature for the Thue-Morse (TMQC) and period-doubling QC (PDQC) with (a,c) $t_A = 0.25$, $t_B = 1$ and (b,d) $t_A = 1$, $t_B = 0.25$. The rest of the parameter values are maintained as in Fig. 1.

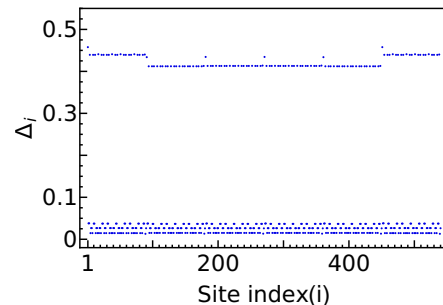


FIG. 14. Distribution of the OP in a 2D Fibonacci QC for $t_v = 0.15$, $t_A = 0.25$, $t_B = 1$. The rest of the parameter values are set as the same in Fig. 1.

illustrated in the main text.

The variation of the entropy and electronic specific heat with temperature for the non-Fibonacci class QC are shown in Fig. 13. For $t_A < t_B$, the period-doubling QC shows a sharp fall in the C_e profile at the transition point, whereas, in the reverse parameter regime $t_A > t_B$, a monotonically increasing behavior of the entropy is observed due to the suppression in OP amplitudes. However, the Thue-Morse QC shows the unusual behavior for both the parameter regimes, as expected due to the branching of the OP following the discussions in the main text.

Appendix C: A few more results of 2D QCs

In this section, we present a few more results on 2D QC to support our conclusion of the present work.

In order to show the effect of the vertical hopping, we show the results of Fibonacci QC for different verti-

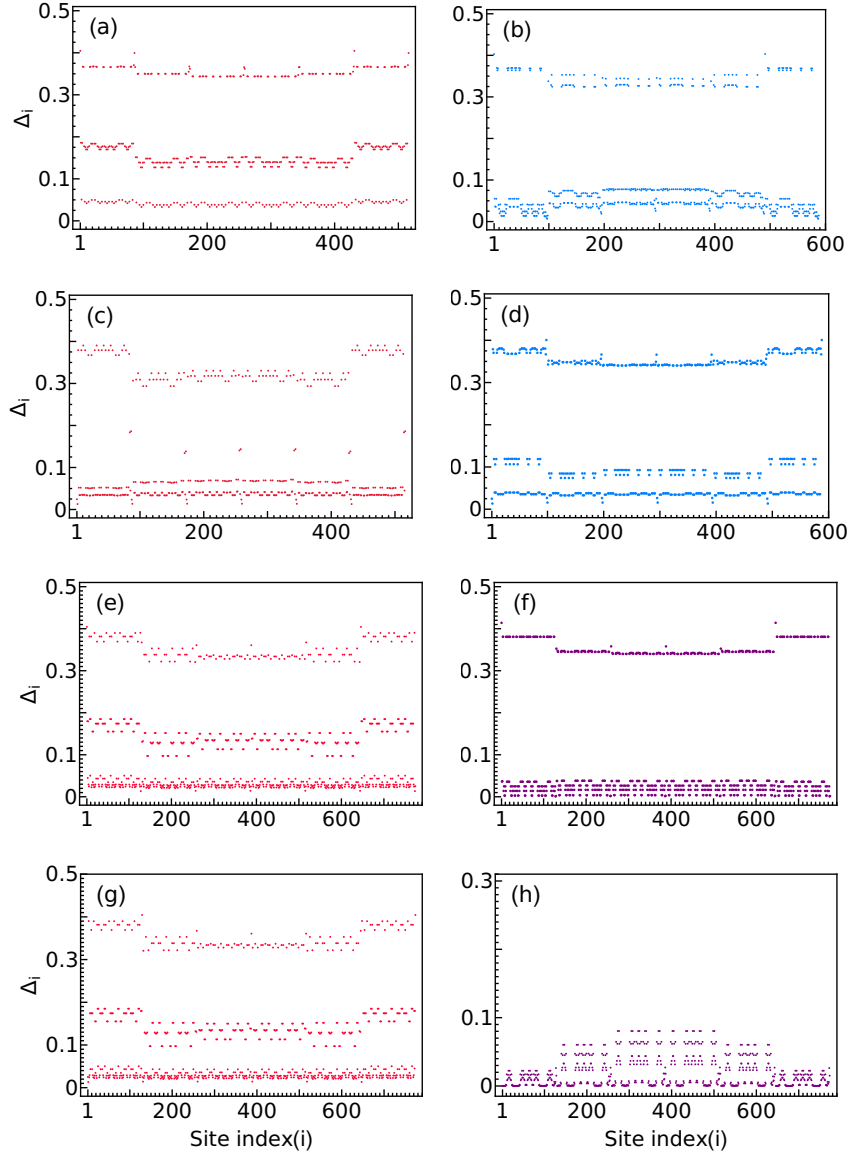


FIG. 15. Distribution of OP over sites for 2D (a,c) Copper-mean, (b,d) Nickel-mean, (e,g) Thue-Morse and (f,h) Period-doubling QC. The hopping amplitudes are taken as (a,b,e,f) $t_A = 0.25$, $t_B = 1$ and (c,d,g,h) $t_A = 1$, $t_B = 0.25$. The vertical hopping strength is set at $t_v = 0.25$. The rest of the parameter values are set as the same in Fig. 1.

cal hopping compared to the main text in Fig. 14. The formation of 2D QC allows three different hopping amplitudes, i.e., t_A , t_B , and t_v . The role of the additional hopping term t_v in 2D case is already discussed. The pairing mechanism becomes stronger with lower t_v magnitudes. As an example, the OP profile for the 2D Fibonacci QC is depicted in Fig. 14 with a lower vertical hopping strength. It exhibits higher magnitudes of OP compared to the previous case where vertical hopping t_v is set equal to t_A (t_B) (see Fig. 9 (a)). This finding is equally applicable to all other 2D QCs for both parameter regimes.

The behavior of OP profiles for 2D GFQC subclass-II family is demonstrated in Fig. 15(a-d). We consider G_7 -th Copper-mean QC containing 516 sites and G_6 -th

Nickel-mean QC containing 588 sites. At the parameter regime $t_A < t_B$, the overall OP distribution breaks into three and two branches for 2D Copper-mean and Nickel-mean QC, respectively (see Fig. 15 (a-b)). Similarly, the OP profiles at reverse regime are depicted in Fig. 15(c-d). So, the overall behavior of the OP landscape is preserved, not affected by the extension in the dimension.

We extend our study to 2D non-Fibonacci QCs to the completeness of the present work. Here also, the 2D OP profiles show similar behavior compared to 1D cases, indicating that the underlying mechanism persists across dimensions. We consider 2D the Thue-Morse and period-doubling QCs in their G_8 -th generation, containing 774 sites. In 2D Thue-Morse QC, the OP profiles are distributed over three branches for both param-

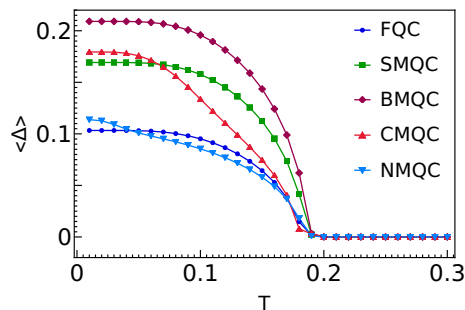


FIG. 16. Variation of average OP with temperature for 2D GFQCs. The parameters are chosen as $t_A = 0.25$, $t_B = 1$, $t_v = 0.25$. The rest of the parameter values are maintained as in Fig. 1 and the abbreviations are the same as in Fig. 4.

eter regimes as shown in Fig. 15(e.g.). Moreover, in 2D period-doubling QC, the OP mainly shows two branches at $t_A < t_B$ (see Fig. 15 (f)). Conversely, in a reverse regime, the OP distribution of 2D period-doubling QC becomes suppressed as depicted in Fig. 15(h). Apart from the distribution of the OP over 2D QC, the temperature dependence of the average OP also shows behavior similar to 1D counterparts. The average OP variation with temperature for 2D GFQC family is shown in Fig. 16 within the parameter regime $t_A < t_B$. Here also at low temperature regime, the Bronze-mean QC exhibits the highest average OP magnitude as seen in the 1D Bronze-mean QC. The behavior of the average OP in these 2D GFQCs in the contrast parameter regime are also very similar to that in 1D GFQCs.

- [1] D. Shechtman, I. Blech, D. Gratias, and J. W. Cahn, “Metallic phase with long-range orientational order and no translational symmetry,” *Phys. Rev. Lett.* **53**, 1951–1953 (1984).
- [2] D. Levine and P. J. Steinhardt, “Quasicrystals: A new class of ordered structures,” *Phys. Rev. Lett.* **53**, 2477–2480 (1984).
- [3] M. Kohmoto, B. Sutherland, and C. Tang, “Critical wave functions and a cantor-set spectrum of a one-dimensional quasicrystal model,” *Phys. Rev. B* **35**, 1020–1033 (1987).
- [4] Y. Liu and R. Riklund, “Electronic properties of perfect and nonperfect one-dimensional quasicrystals,” *Phys. Rev. B* **35**, 6034–6042 (1987).
- [5] T. Fujiwara, M. Kohmoto, and T. Tokihiro, “Multifractal wave functions on a fibonacci lattice,” *Phys. Rev. B* **40**, 7413–7416 (1989).
- [6] N. Macé, A. Jagannathan, and F. Piéchon, “Fractal dimensions of wave functions and local spectral measures on the fibonacci chain,” *Phys. Rev. B* **93**, 205153 (2016).
- [7] C. S. Ryu, G. Y. Oh, and M. H. Lee, “Electronic properties of a tight-binding and a kronig-penney model of the thue-morse chain,” *Phys. Rev. B* **48**, 132–141 (1993).
- [8] Q. Niu and F. Nori, “Renormalization-group study of one-dimensional quasiperiodic systems,” *Phys. Rev. Lett.* **57**, 2057–2060 (1986).
- [9] E. Maciá and F. Domínguez-Adame, “Physical nature of critical wave functions in fibonacci systems,” *Phys. Rev. Lett.* **76**, 2957–2960 (1996).
- [10] X. Fu, Y. Liu, B. Cheng, and D. Zheng, “Spectral structure of two-dimensional fibonacci quasilattices,” *Phys. Rev. B* **43**, 10808–10814 (1991).
- [11] L. Kroon, E. Lennholm, and R. Riklund, “Localization-delocalization in aperiodic systems,” *Phys. Rev. B* **66**, 094204 (2002).
- [12] R. B. Capaz, B. Koiller, and S. L. A. de Queiroz, “Gap states and localization properties of one-dimensional fibonacci quasicrystals,” *Phys. Rev. B* **42**, 6402–6407 (1990).
- [13] A. Jagannathan, “The fibonacci quasicrystal: Case study of hidden dimensions and multifractality,” *Rev. Mod. Phys.* **93**, 045001 (2021).
- [14] N. Macé, A. Jagannathan, P. Kalugin, R. Mosseri, and F. Piéchon, “Critical eigenstates and their properties in one- and two-dimensional quasicrystals,” *Phys. Rev. B* **96**, 045138 (2017).
- [15] E. Maciá, “Physical nature of critical modes in fibonacci quasicrystals,” *Phys. Rev. B* **60**, 10032–10036 (1999).
- [16] R. Merlin, K. Bajema, R. Clarke, F. Y. Juang, and P. K. Bhattacharya, “Quasiperiodic gaas-alas heterostructures,” *Phys. Rev. Lett.* **55**, 1768–1770 (1985).
- [17] V. Elser and C. L. Henley, “Crystal and quasicrystal structures in al-mn-si alloys,” *Phys. Rev. Lett.* **55**, 2883–2886 (1985).
- [18] J. Todd, R. Merlin, R. Clarke, K. M. Mohanty, and J. D. Axe, “Synchrotron x-ray study of a fibonacci superlattice,” *Phys. Rev. Lett.* **57**, 1157–1160 (1986).
- [19] L. X. He, X. Z. Li, Z. Zhang, and K. H. Kuo, “One-dimensional quasicrystal in rapidly solidified alloys,” *Phys. Rev. Lett.* **61**, 1116–1118 (1988).
- [20] R. Merlin, K. Bajema, J. Nagle, and K. Ploog, “Raman scattering by acoustic phonons and structural properties of fibonacci, thue-morse and random superlattices,” *Le Journal de Physique Colloques* **48**, C5–503 (1987).
- [21] D. Mayou, C. Berger, F. Cyrot-Lackmann, T. Klein, and P. Lanco, “Evidence for unconventional electronic transport in quasicrystals,” *Phys. Rev. Lett.* **70**, 3915–3918 (1993).
- [22] J. E. Zárate and V. R. Velasco, “Electronic properties of quasiperiodic heterostructures,” *Phys. Rev. B* **65**, 045304 (2001).
- [23] L. Dal Negro, M. Stolfi, Y. Yi, J. Michel, X. Duan, L. Kimerling, J. LeBlanc, and J. Haavisto, “Photon band gap properties and omnidirectional reflectance in si/ sio2 thue-morse quasicrystals,” *Applied Phys. Lett.* **84**, 5186–5188 (2004).
- [24] A. Yamamoto, “Section method for projected structures of icosahedral quasicrystals and its application to electron-microscopy-image and surface analyses,” *Phys. Rev. Lett.* **93**, 195505 (2004).
- [25] J. Hendrickson, B. C. Richards, J. Sweet, G. Khitrova, A. N. Poddubny, E. L. Ivchenko, M. Wegener, and H. M. Gibbs, “Excitonic polaritons in fibonacci quasicrystals,” *Opt. Express* **16**, 15382–15387 (2008).
- [26] V. Passias, N. V. Valappil, Z. Shi, L. Deych, A. A. Lisiansky, and V. M. Menon, “Luminescence proper-

- ties of a fibonacci photonic quasicrystal,” *Opt. Express* **17**, 6636–6642 (2009).
- [27] K. Nagao, T. Inuzuka, K. Nishimoto, and K. Edagawa, “Experimental observation of quasicrystal growth,” *Phys. Rev. Lett.* **115**, 075501 (2015).
- [28] M. Mihalkovič and M. Widom, “Spontaneous formation of thermodynamically stable al-cu-fe icosahedral quasicrystal from realistic atomistic simulations,” *Phys. Rev. Res.* **2**, 013196 (2020).
- [29] M. Reisner, Y. Tahmi, F. Piéchon, U. Kuhl, and F. Mortessagne, “Experimental observation of multifractality in fibonacci chains,” *Phys. Rev. B* **108**, 064210 (2023).
- [30] F. E. Wüthrl, O. Krahn, S. Schenk, W. Widdra, and S. Förster, “Quasicrystal approximants in the two-dimensional ba-ti-o system on pd(111): A leed, xps, and stm study,” *Phys. Rev. B* **107**, 195414 (2023).
- [31] G. Y. Oh and M. H. Lee, “Band-structural and fourier-spectral properties of one-dimensional generalized fibonacci lattices,” *Phys. Rev. B* **48**, 12465–12477 (1993).
- [32] M. Kolář, M. K. Ali, and F. Nori, “Generalized thue-morse chains and their physical properties,” *Phys. Rev. B* **43**, 1034–1047 (1991).
- [33] Z. Cheng, R. Savit, and R. Merlin, “Structure and electronic properties of thue-morse lattices,” *Phys. Rev. B* **37**, 4375–4382 (1988).
- [34] S. Chattopadhyay, A. Ghosh, and A. Chakrabarti, “Frequency dependent response of a thue-morse aperiodic lattice,” *Phys. Rev. B* **63**, 064201 (2001).
- [35] P. Carpena, V. Gasparian, and M. Ortuño, “Energy spectra and level statistics of fibonacci and thue-morse chains,” *Phys. Rev. B* **51**, 12813–12816 (1995).
- [36] V. Velasco, “Electronic properties of fibonacci quasiperiodic heterostructures,” *Microelectronics Journal* **33**, 361–364 (2002).
- [37] W. M. Zheng, “Global scaling properties of the spectrum for the fibonacci chains,” *Phys. Rev. A* **35**, 1467–1469 (1987).
- [38] Q. Niu and F. Nori, “Spectral splitting and wavefunction scaling in quasicrystalline and hierarchical structures,” *Phys. Rev. B* **42**, 10329–10341 (1990).
- [39] F. Piéchon, M. Benakli, and A. Jagannathan, “Analytical results for scaling properties of the spectrum of the fibonacci chain,” *Phys. Rev. Lett.* **74**, 5248–5251 (1995).
- [40] A. Chakrabarti, R. A. Römer, and M. Schreiber, “Magnetotransport in periodic and quasiperiodic arrays of mesoscopic rings,” *Phys. Rev. B* **68**, 195417 (2003).
- [41] A. Mordret and A. G. Grushin, “Beating the aliasing limit with aperiodic monotile arrays,” *Phys. Rev. Appl.* **23**, 034021 (2025).
- [42] J. Schirmann, S. Franca, F. Flicker, and A. G. Grushin, “Physical properties of an aperiodic monotile with graphene-like features, chirality, and zero modes,” *Phys. Rev. Lett.* **132**, 086402 (2024).
- [43] P. Dutta, S. K. Maiti, and S. Karmakar, “A renormalization group study of persistent current in a quasiperiodic ring,” *Physics Letters A* **378**, 1388–1391 (2014).
- [44] S. Das Sarma and X. C. Xie, “Conductance fluctuations in one-dimensional quasicrystals,” *Phys. Rev. B* **37**, 1097–1102 (1988).
- [45] M. Röntgen, C. V. Morfonios, R. Wang, L. Dal Negro, and P. Schmelcher, “Local symmetry theory of resonator structures for the real-space control of edge states in binary aperiodic chains,” *Phys. Rev. B* **99**, 214201 (2019).
- [46] T. Matsubara, A. Koga, and T. Dotera, “Triangular and dice quasicrystals modulated by generic one-dimensional aperiodic sequences,” *Phys. Rev. B* **111**, 104104 (2025).
- [47] J. M. Luck, “Cantor spectra and scaling of gap widths in deterministic aperiodic systems,” *Phys. Rev. B* **39**, 5834–5849 (1989).
- [48] A. Chakrabarti and S. N. Karmakar, “Renormalization-group method for exact green’s functions of self-similar lattices: Application to generalized fibonacci chains,” *Phys. Rev. B* **44**, 896–899 (1991).
- [49] S. Sil, S. N. Karmakar, R. K. Moitra, and A. Chakrabarti, “Extended states in one-dimensional lattices: Application to the quasiperiodic copper-mean chain,” *Phys. Rev. B* **48**, 4192–4195 (1993).
- [50] C. S. Ryu, G. Y. Oh, and M. H. Lee, “Extended and critical wave functions in a thue-morse chain,” *Phys. Rev. B* **46**, 5162–5168 (1992).
- [51] A. Ghosh and S. N. Karmakar, “Trace map of a general aperiodic thue-morse chain: Electronic properties,” *Phys. Rev. B* **58**, 2586–2590 (1998).
- [52] G. Gumbs, G. S. Dubey, A. Salman, B. S. Mahmoud, and D. Huang, “Statistical and transport properties of quasiperiodic layered structures: Thue-morse and fibonacci,” *Phys. Rev. B* **52**, 210–219 (1995).
- [53] F. Nori and J. P. Rodriguez, “Acoustic and electronic properties of one-dimensional quasicrystals,” *Phys. Rev. B* **34**, 2207–2211 (1986).
- [54] M. Kohmoto and J. R. Banavar, “Quasiperiodic lattice: Electronic properties, phonon properties, and diffusion,” *Phys. Rev. B* **34**, 563–566 (1986).
- [55] K. Lambropoulos and C. Simserides, “Periodic, quasiperiodic, fractal, kolakoski, and random binary polymers: Energy structure and carrier transport,” *Phys. Rev. E* **99**, 032415 (2019).
- [56] M. Dulea, M. Johansson, and R. Riklund, “Localization of electrons and electromagnetic waves in a deterministic aperiodic system,” *Phys. Rev. B* **45**, 105–114 (1992).
- [57] D. E. Katsanos, S. N. Evangelou, and S. J. Xiong, “Quantum electron dynamics in periodic and aperiodic sequences,” *Phys. Rev. B* **51**, 895–904 (1995).
- [58] P. E. de Brito, C. A. A. da Silva, and H. N. Nazareno, “Field-induced localization in fibonacci and thue-morse lattices,” *Phys. Rev. B* **51**, 6096–6099 (1995).
- [59] E. Diez, F. Domínguez-Adame, E. Maciá, and A. Sánchez, “Dynamical phenomena in fibonacci semiconductor superlattices,” *Phys. Rev. B* **54**, 16792–16798 (1996).
- [60] F. Piéchon, “Anomalous diffusion properties of wave packets on quasiperiodic chains,” *Phys. Rev. Lett.* **76**, 4372–4375 (1996).
- [61] R. Ketzmerick, K. Kruse, S. Kraut, and T. Geisel, “What determines the spreading of a wave packet?” *Phys. Rev. Lett.* **79**, 1959–1963 (1997).
- [62] C. Chiaracane, F. Pietracaprina, A. Purkayastha, and J. Goold, “Quantum dynamics in the interacting fibonacci chain,” *Phys. Rev. B* **103**, 184205 (2021).
- [63] S. Thiem, M. Schreiber, and U. Grimm, “Wave packet dynamics, ergodicity, and localization in quasiperiodic chains,” *Phys. Rev. B* **80**, 214203 (2009).
- [64] S. Biswas and A. Chakrabarti, “Engineering complete delocalization of single particle states in a class of one dimensional aperiodic lattices: A quantum dynamical

- cal study,” *Physica E: Low-dimensional Systems and Nanostructures* **162**, 116010 (2024).
- [65] Y. E. Kraus, Y. Lahini, Z. Ringel, M. Verbin, and O. Zilberberg, “Topological states and adiabatic pumping in quasicrystals,” *Phys. Rev. Lett.* **109**, 106402 (2012).
- [66] S. Longhi, “Topological phase transition in non-hermitian quasicrystals,” *Phys. Rev. Lett.* **122**, 237601 (2019).
- [67] Q. Lin, T. Li, L. Xiao, K. Wang, W. Yi, and P. Xue, “Topological phase transitions and mobility edges in non-hermitian quasicrystals,” *Phys. Rev. Lett.* **129**, 113601 (2022).
- [68] R. Chen, D.-H. Xu, and B. Zhou, “Topological anderson insulator phase in a quasicrystal lattice,” *Phys. Rev. B* **100**, 115311 (2019).
- [69] R. Chen, B. Zhou, and D.-H. Xu, “Quasicrystalline second-order topological semimetals,” *Phys. Rev. B* **108**, 195306 (2023).
- [70] C. Rangi, K.-M. Tam, and J. Moreno, “Engineering a non-hermitian second-order topological insulator state in quasicrystals,” *Phys. Rev. B* **109**, 064203 (2024).
- [71] F. Baboux, E. Levy, A. Lemaitre, C. Gómez, E. Galopin, L. Le Gratiet, I. Sagnes, A. Amo, J. Bloch, and E. Akkermans, “Measuring topological invariants from generalized edge states in polaritonic quasicrystals,” *Phys. Rev. B* **95**, 161114 (2017).
- [72] T. Peng, Y.-C. Xiong, C.-B. Hua, Z.-R. Liu, X. Zhu, W. Cao, F. Lv, Y. Hou, B. Zhou, Z. Wang, and R. Xiong, “Structural disorder-induced topological phase transitions in quasicrystals,” *Phys. Rev. B* **109**, 195301 (2024).
- [73] R. Chen, C.-Z. Chen, J.-H. Gao, B. Zhou, and D.-H. Xu, “Higher-order topological insulators in quasicrystals,” *Phys. Rev. Lett.* **124**, 036803 (2020).
- [74] H. Huang and F. Liu, “Comparison of quantum spin hall states in quasicrystals and crystals,” *Phys. Rev. B* **100**, 085119 (2019).
- [75] M. Verbin, O. Zilberberg, Y. E. Kraus, Y. Lahini, and Y. Silberberg, “Observation of topological phase transitions in photonic quasicrystals,” *Phys. Rev. Lett.* **110**, 076403 (2013).
- [76] C. Ouyang, Q. He, D.-H. Xu, and F. Liu, “Higher-order topology in fibonacci quasicrystals,” *Phys. Rev. B* **110**, 075425 (2024).
- [77] C. W. Duncan, S. Manna, and A. E. B. Nielsen, “Topological models in rotationally symmetric quasicrystals,” *Phys. Rev. B* **101**, 115413 (2020).
- [78] Z.-G. Chen, C. Lou, K. Hu, and L.-K. Lim, “Fractal surface states in three-dimensional topological quasicrystals,” *Phys. Rev. Res.* **6**, 043054 (2024).
- [79] C. Wang, F. Liu, and H. Huang, “Effective model for fractional topological corner modes in quasicrystals,” *Phys. Rev. Lett.* **129**, 056403 (2022).
- [80] K. Kamiya, T. Takeuchi, N. Kabeya, N. Wada, T. Ishimasa, A. Ochiai, K. Deguchi, K. Imura, and N. Sato, “Discovery of superconductivity in quasicrystal,” *Nature communications* **9**, 154 (2018).
- [81] M. Sun, T. Čadež, I. Yurkevich, and A. Andreanov, “Enhancement of superconductivity in the fibonacci chain,” *Phys. Rev. B* **109**, 134504 (2024).
- [82] Y. Wang, G. Rai, C. Matsumura, A. Jagannathan, and S. Haas, “Superconductivity in the fibonacci chain,” *Phys. Rev. B* **109**, 214507 (2024).
- [83] A. Sandberg, O. A. Awoga, A. M. Black-Schaffer, and P. Holmval, “Josephson effect in a fibonacci quasicrystal,” *Phys. Rev. B* **110**, 104513 (2024).
- [84] A. Kobialka, O. A. Awoga, M. Leijnse, T. Domański, P. Holmval, and A. M. Black-Schaffer, “Topological superconductivity in fibonacci quasicrystals,” *Phys. Rev. B* **110**, 134508 (2024).
- [85] G. Rai, S. Haas, and A. Jagannathan, “Proximity effect in a superconductor-quasicrystal hybrid ring,” *Phys. Rev. B* **100**, 165121 (2019).
- [86] G. Rai, S. Haas, and A. Jagannathan, “Superconducting proximity effect and order parameter fluctuations in disordered and quasiperiodic systems,” *Phys. Rev. B* **102**, 134211 (2020).
- [87] R. Ghadimi, T. Sugimoto, K. Tanaka, and T. Tohyama, “Topological superconductivity in quasicrystals,” *Phys. Rev. B* **104**, 144511 (2021).
- [88] R. N. Araújo and E. C. Andrade, “Conventional superconductivity in quasicrystals,” *Phys. Rev. B* **100**, 014510 (2019).
- [89] S. Sakai, N. Takemori, A. Koga, and R. Arita, “Superconductivity on a quasiperiodic lattice: Extended-to-localized crossover of cooper pairs,” *Phys. Rev. B* **95**, 024509 (2017).
- [90] L. Liu, Z.-X. Li, and F. Yang, “Superconductivity and charge density wave in the holstein model on the penrose lattice,” *Phys. Rev. Lett.* **134**, 206001 (2025).
- [91] M. Hori, T. Sugimoto, T. Tohyama, and K. Tanaka, “Self-consistent study of topological superconductivity in two-dimensional quasicrystals,” *Phys. Rev. B* **110**, 144512 (2024).
- [92] D. Pines, “Superconductivity in the periodic system,” *Phys. Rev.* **109**, 280–287 (1958).
- [93] A. Ghosal, M. Randeria, and N. Trivedi, “Inhomogeneous pairing in highly disordered s-wave superconductors,” *Phys. Rev. B* **65**, 014501 (2001).
- [94] K. Tanaka and F. Marsiglio, “Anderson prescription for surfaces and impurities,” *Phys. Rev. B* **62**, 5345–5348 (2000).
- [95] L. Yin, Y. Bai, M. Zhang, A. A. Shanenko, and Y. Chen, “Surface superconductor-insulator transition induced by electric field,” *Phys. Rev. B* **108**, 054508 (2023).
- [96] A. Ghosal, M. Randeria, and N. Trivedi, “Spatial inhomogeneities in disordered d-wave superconductors,” *Phys. Rev. B* **63**, 020505 (2000).
- [97] M. D. Croitoru, A. A. Shanenko, Y. Chen, A. Vagov, and J. A. Aguiar, “Microscopic description of surface superconductivity,” *Phys. Rev. B* **102**, 054513 (2020).
- [98] Y. Bai, Y. Chen, M. D. Croitoru, A. A. Shanenko, X. Luo, and Y. Zhang, “Interference-induced surface superconductivity: Enhancement by tuning the debye energy,” *Phys. Rev. B* **107**, 024510 (2023).
- [99] Y. Bai, L. Zhang, X. Luo, A. A. Shanenko, and Y. Chen, “Tailoring of interference-induced surface superconductivity by an applied electric field,” *Phys. Rev. B* **108**, 134506 (2023).
- [100] W.-C. Chen, Y. Wang, and C.-C. Chen, “Superconducting phases of the square-lattice extended hubbard model,” *Phys. Rev. B* **108**, 064514 (2023).
- [101] Y. Chen, K.-J. Chen, J.-J. Zhu, and A. A. Shanenko, “Emergence of surface superconductivity through interference in proximitized topological insulators,” *Phys. Rev. B* **109**, 224514 (2024).

- [102] D. Chakraborty, R. Sensarma, and A. Ghosal, “Effects of strong disorder in strongly correlated superconductors,” *Phys. Rev. B* **95**, 014516 (2017).
- [103] Y. Wang, G. Rai, S. Haas, and A. Jagannathan, “Edge and corner superconductivity in a two-dimensional topological model,” *Phys. Rev. B* **107**, 104507 (2023).
- [104] K. Aryanpour, E. R. Dagotto, M. Mayr, T. Paiva, W. E. Pickett, and R. T. Scalettar, “Effect of inhomogeneity on s -wave superconductivity in the attractive hubbard model,” *Phys. Rev. B* **73**, 104518 (2006).
- [105] E. M. Barber, *Aperiodic Structures in Condensed Matter: Fundamentals and Applications*, 1st ed. (CRC Press, Boca Raton, 2008).
- [106] E. Maciá, “Spectral classification of one-dimensional binary aperiodic crystals: An algebraic approach,” *Annalen der Physik* **529**, 1700079 (2017).
- [107] E. Maciá, “The role of aperiodic order in science and technology,” *Reports on Progress in Physics* **69**, 397 (2005).
- [108] P.-G. De Gennes, *Superconductivity of metals and alloys* (CRC press, 2018).
- [109] B. P. Stojković and O. T. Valls, “Order parameter near a superconductor-insulator interface,” *Phys. Rev. B* **47**, 5922–5930 (1993).
- [110] R. J. Troy and A. T. Dorsey, “Self-consistent microscopic theory of surface superconductivity,” *Phys. Rev. B* **51**, 11728–11732 (1995).
- [111] A. M. Martin and J. F. Annett, “Self-consistent interface properties of d - and s -wave superconductors,” *Phys. Rev. B* **57**, 8709–8716 (1998).
- [112] A. A. Shanenko and M. D. Croitoru, “Shape resonances in the superconducting order parameter of ultrathin nanowires,” *Phys. Rev. B* **73**, 012510 (2006).
- [113] Z. V. Vardeny, A. Nahata, and A. Agrawal, “Optics of photonic quasicrystals,” *Nature photonics* **7**, 177–187 (2013).
- [114] V. Matarazzo, S. De Nicola, G. Zito, P. Mormile, M. Ripa, G. Abbate, J. Zhou, and L. Petti, “Spectral characterization of two-dimensional thue–morse quasicrystals realized with high resolution lithography,” *Journal of Optics* **13**, 015602 (2010).
- [115] G. Zito, B. Piccirillo, E. Santamato, A. Marino, V. Tkachenko, and G. Abbate, “Two-dimensional photonic quasicrystals by single beam computer-generated holography,” *Opt. Express* **16**, 5164–5170 (2008).
- [116] T. Takeuchi and U. Mizutani, “Electronic structure, electron transport properties, and relative stability of icosahedral quasicrystals and their 1/1 and 2/1 approximants in the al-mg-zn alloy system,” *Phys. Rev. B* **52**, 9300–9309 (1995).
- [117] M. Windisch, M. Krajci, and J. Hafner, “Electronic structure in icosahedral alcu quasicrystals and approximant crystals,” *Journal of Physics: Condensed Matter* **6**, 6977 (1994).
- [118] U. Mizutani, T. Matsuda, Y. Itoh, K. Tanaka, H. Domae, T. Mizuno, S. Murasaki, Y. Miyoshi, K. Hashimoto, and Y. Yamada, “Electronic structure and electron transport properties of quasicrystals and approximant crystals in al tm and mg ga al zn alloy systems,” *Journal of Non-Crystalline Solids* **156-158**, 882–886 (1993).
- [119] M. Saito, T. Sekikawa, and Y. Ōno, “Electronic states of al–mg–zn quasicrystal and its approximant based on first-principles calculations,” *physica status solidi (b)* **257**, 2000108 (2020).
- [120] S.-y. Li, Z. Xu, Y. Wang, Y. Han, K. Watanabe, T. Taniguchi, A. Song, T.-B. Ma, H.-J. Gao, Y. Jiang, and J. Mao, “Quasiperiodic moiré reconstruction and modulation of electronic properties in twisted bilayer graphene aligned with hexagonal boron nitride,” *Phys. Rev. Lett.* **133**, 196401 (2024).
- [121] N. Wang, H. Chen, and K. H. Kuo, “Two-dimensional quasicrystal with eightfold rotational symmetry,” *Phys. Rev. Lett.* **59**, 1010–1013 (1987).
- [122] V. Kumar, D. Sahoo, and G. Athithan, “Characterization and decoration of the two-dimensional penrose lattice,” *Phys. Rev. B* **34**, 6924–6932 (1986).
- [123] M. M. A. Ezzi, G. N. Pallewela, C. De Beule, E. J. Mele, and S. Adam, “Analytical model for atomic relaxation in twisted moiré materials,” *Phys. Rev. Lett.* **133**, 266201 (2024).
- [124] M. Gierer, M. A. Van Hove, A. I. Goldman, Z. Shen, S.-L. Chang, P. J. Pinhero, C. J. Jenks, J. W. Anderegg, C.-M. Zhang, and P. A. Thiel, “Fivefold surface of quasicrystalline alpdmm: Structure determination using low-energy-electron diffraction,” *Phys. Rev. B* **57**, 7628–7641 (1998).
- [125] J. A. Smerdon, J. K. Parle, L. H. Wearing, T. A. Lograsso, A. R. Ross, and R. McGrath, “Nucleation and growth of a quasicrystalline monolayer: Bi adsorption on the fivefold surface of i -al₇₀pd₂₁mn₉,” *Phys. Rev. B* **78**, 075407 (2008).
- [126] Y. Iwasaki, K. Kitahara, and K. Kimura, “Effects of cu doping on thermoelectric properties of al–si–ru semiconducting quasicrystalline approximant,” *Phys. Rev. Mater.* **5**, 125401 (2021).
- [127] K. Hayashida, T. Dotera, A. Takano, and Y. Matsushita, “Polymeric quasicrystal: Mesoscopic quasicrystalline tiling in abc star polymers,” *Phys. Rev. Lett.* **98**, 195502 (2007).
- [128] Y. Chen, Q. Zhu, M. Zhang, X. Luo, and A. Shanenko, “Surface superconductor-insulator transition: Reduction of the critical electric field by hartree-fock potential,” *Physics Letters A* **494**, 129281 (2024).